Characterizing Spatial and Temporal Changes in Kansas's Seasonal to Annual Hydroclimatic Extremes

Authors: Sam Zipper[1,2,*], Archi Howlader[1], David Weiss[3,4], Jude Kastens[3], Erin Seybold[1,2]

1. Kansas Geological Survey, University of Kansas
2. Department of Geology, University of Kansas
3. Kansas Biological Survey & Center for Ecological Research, University of Kansas
4. Department of Geography & Atmospheric Science, University of Kansas

* Correspondence to Sam Zipper, samzipper@ku.edu

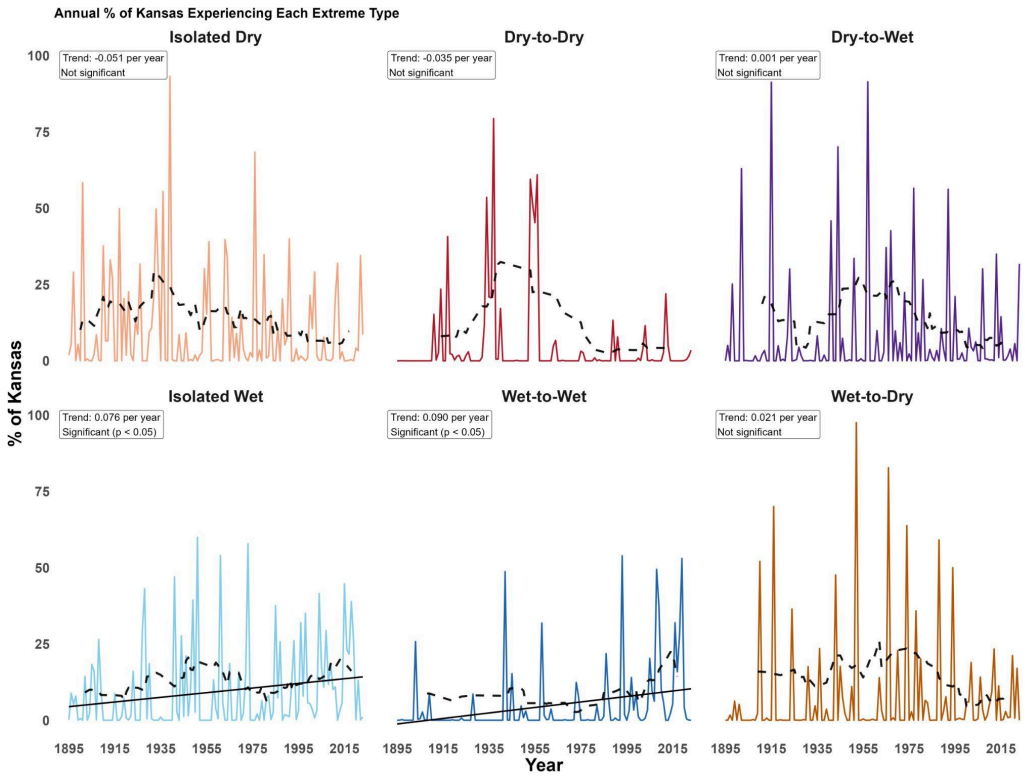

Kansas Geological Survey Open-File Report 2026-34

Funding: This work was primarily funded by Kansas Water Office contracts nos. 25-113 and 25-132. Additional support was provided by the U.S. Department of Agriculture, National Institute of Food and Agriculture, Agriculture and Food Research Initiative (USDA NIFA AFRI), Water Quantity and Quality program grant no. 2022–67019-38447.

Table of Contents

Executive Summary

Hydroclimatic extremes, such as droughts and floods, are key stress points for water management across diverse sectors (water treatment, reservoir operations, agriculture, etc.). Unfortunately, climate models struggle to predict extremes, and therefore understanding historical trajectories of change may offer one of the best clues for how hydroclimatic extremes may persist or change in the future for Kansas and the broader Great Plains region. Uncertainty increases even further when considering compound hydroclimatic extremes, such as recurring extreme conditions (e.g., consecutive wetter-than-average years in 1985 and 1986 that led to widespread flooding) and "weather whiplash" such as transitions from anomalously wet to anomalously dry conditions (as observed from 2018 to 2019) or vice versa. The goal of this project was to better understand historical patterns and trends in seasonal to annual hydroclimatic extremes in Kansas, including compound extremes. Specifically, we had three objectives:

Objective 1: Quantify spatiotemporal patterns in seasonal to annual hydroclimatic extremes.

We compiled historical precipitation data from both meteorological stations and the gridded Parameter-elevation Regressions on Independent Slopes Model (PRISM) dataset for Kansas as well as areas outside of Kansas that contribute to the state's federal reservoirs. Because gridded products sometimes struggle to identify extremes at daily resolution, we first compared these two data sources, finding that PRISM was able to accurately reproduce annual and seasonal precipitation totals, and associated identification of extremes, with a maximum annual bias of approximately 5% for dry-to-dry event identification and no seasonal bias exceeding 10%. Based on this, we selected PRISM to use for historical statewide analysis because it is gap-free in space and time. We obtained PRISM data for a 128-year period (1895–2023) and calculated seasonal and annual precipitation depths for each year. We then developed a percentile-based approach to identify seasonal and annual hydroclimatic extremes, with six different extreme types: isolated wet or dry conditions, defined as a wet or dry period not preceded by a different extreme; recurring wet or dry (referred to as wet-to-wet and dry-to-dry), defined as a wet or dry extremes preceded by an extreme of the same type; and whiplash wet-to-dry or dry-to-wet transitions, defined based on a change in percentile of at least 60 points between years (for annual analysis) or seasons (for seasonal analysis). This produced a 4 km resolution database of seasonal and annual precipitation and a classification of precipitation extremes for our study domain. To contextualize the extreme analysis, we also calculated long-term annual and seasonal precipitation trends.

Objective 2: Analyze changes in hydroclimatic extremes in different water management areas.

Using this database, we then investigated spatial and temporal patterns of precipitation and precipitation extremes for the past 128 years. Annual precipitation is increasing across much of the state, with significant long-term wetting trends over 40.3% of Kansas, including most of the central and eastern portions of the state. These increasing precipitation trends are primarily

driven by spring rainfall increases. We analyzed precipitation extremes on a gridded basis and summarized for 148 state-relevant water management areas, including contributing areas to federal reservoirs in the state, groundwater management districts (GMDs), and Regional Advisory Committee (RAC) boundaries. Our analysis found that both isolated wet and recurring wet-to-wet extremes have become significantly more widespread in Kansas, particularly since about 1980, consistent with increases in annual precipitation. For discussion in this report, we primarily focus on contributing areas of Kansas's reservoirs. Western reservoirs exhibit persistent drying tendencies while eastern reservoirs show increasingly wet conditions. Whiplash events, defined as rapid transitions between wet and dry conditions, occur most frequently during summer and are more common in northern and eastern reservoirs. Seasonal patterns indicate strong spring wetness, drying tendencies in fall, and generally dry conditions in winter. We show that the number of wet extremes occurring since a reservoir was created is significantly correlated with the overall loss in reservoir capacity, though this may be confounded by the fact that reservoirs exposed to more extremes could have been constructed earlier.

Objective 3: Develop an interactive, web-based tool for Kansas's hydroclimatic extremes.

To support the exploration and dissemination of project results, we developed an interactive, web-based application. The tool summarizes data for 148 management-relevant boundaries within the state: 24 federal reservoir watersheds, 5 GMDs, 14 RAC boundaries, and 105 counties. Because of the spatial nature of the analysis, we designed the tool around an interactive map interface on the ESRI Experience Builder platform. The tool allows users to select a particular boundary, explore pre-made visualizations of historical precipitation and extremes, and download the data for integration with other data products. The tool is available online at https://kars.ku.edu/pages/hydroclimate-extremes

Conclusions and Implications

The findings from this project show that much of Kansas, including most of the central and eastern portions of the state, experienced significant increases in precipitation over the past 120 years. Coincident with these increases in annual precipitation, wet extremes are becoming significantly more common. Increases in precipitation and wet extremes have been most significant in the spring (March-May) and accelerated over the past 40 years. Due to these regional patterns, most reservoirs in the central and eastern portion of the state have been exposed to more wet extremes than dry extremes in the recent past, and wet extreme occurrence is significantly associated with a loss of reservoir storage capacity. Further evaluation of changes in evapotranspiration (ET) are necessary to determine whether Kansas has become drier or wetter overall as a result of these precipitation changes. This work contributes to the pillars of the Kansas Water Plan through the improved characterization of seasonal to annual hydroclimatic extremes and the creation of a web tool to increase awareness of Kansas water resources for reservoirs, RACs, GMDs, and counties across the state.

Introduction

Hydroclimatic extremes, such as droughts and floods, are stress points for water management. Extremes can have many negative impacts, including socio-economic devastation (Fraser, 2013; Kuil et al., 2016), reduced agricultural production (Houspanossian et al., 2023; Reyes et al., 2020), soil loss (Bolles and Forman, 2018), stream drying (Datry et al., 2022; Zipper et al., 2021, 2022), ecological degradation (Perkin et al., 2019; Rogosch et al., 2019) and water shortages (Di Baldassarre et al., 2018). Compound extremes, in which multiple extremes (dry or wet) happen concurrently or in sequence, are even more stressful (He and Sheffield, 2020; Na and Najafi, 2024). Compound extremes can be recurring, such as consecutive years of drought or high precipitation, and have cumulative effects that exacerbate negative impacts relative to a single year of isolated extreme conditions. Whiplash extremes, characterized by rapid transitions between wet and dry conditions (Fu et al., 2025; Loecke et al., 2017; Swain et al., 2025), also can be particularly disruptive, as systems designed to cope with one extreme may struggle to adjust to the opposite condition (Na and Najafi, 2024). The intensification of the water cycle, driven in part by climate change, is thought to lead to increasing hydroclimatic extremes worldwide (Di Capua and Rahmstorf, 2023; Easterling et al., 2016; Gründemann et al., 2023), and future projections suggest that they will continue to intensify (Fowler et al., 2022; Swain et al., 2025; Yuan et al., 2023).

Climate models often struggle to predict extremes, and therefore understanding historical trajectories of change may offer one of the best clues for how precipitation extremes may persist or vary in the future. There is strong regional variability in when and how precipitation extremes have changed historically. Past studies showed an increase in frequency and severity of precipitation extremes, such as floods and droughts, over many North American catchments (Zhao et al., 2020). In tropical regions, precipitation extremes are predominant during the monsoon period, which has been prolonged in recent decades (Kitoh et al., 2013). On the other hand, the mid-latitudes experience substantial precipitation during transitional seasons, which are shifting to earlier in the year in places (Tramblay et al., 2023). A recent study found that the frequency of planetary wave resonance events, which are atmospheric circulation features linked to extreme summer weather, has tripled since the 1950s (Li et al., 2025), a trend that current climate models struggle to capture. This points to significant gaps in how models handle atmospheric dynamics and persistent extreme conditions such as droughts and floods.

Given the importance of hydroclimatic extremes to water management and challenges in forecasting their future occurrence, this project's goal was to better understand historical patterns and trends in seasonal to annual hydroclimatic extremes in Kansas, including compound extremes, and develop a user-friendly tool to visualize these patterns. Our objectives were to:

1. Quantify spatiotemporal patterns in seasonal to annual hydroclimatic extremes.
2. Analyze changes in hydroclimatic extremes in different water management areas.
3. Develop an interactive, web-based tool for Kansas's hydroclimatic extremes.

This report describes methods, outcomes, and findings from each objective.

Objective 1: Quantify spatiotemporal patterns in seasonal to annual hydroclimatic extremes

1.1 Extreme classification

To investigate changes in different types of hydroclimatic extremes through time and space, we developed six mutually exclusive extreme typologies (Figure 1). These categories included isolated extremes (dry or wet) that were not preceded by another extreme type; recurring extremes (dry-to-dry or wet-to-wet) in which an extreme followed an extreme of the same type; and whiplash extremes (dry-to-wet or wet-to-dry) in which an extreme occurred after a large shift from the opposite type of hydroclimatic conditions. We used a percentile-based approach, rather than absolute precipitation depth thresholds, to identify extremes so that our method would be scalable across both space (spanning a wide range of climates in Kansas) and time (to work at both annual and seasonal timescales), as in Swain et al., 2018. To classify extremes, monthly precipitation was summed to obtain a seasonal or annual total, and extremes were identified as follows:

- Isolated dry = precipitation is lower than the 20th percentile and previous timestep precipitation was greater than 20th percentile & change from previous timestep did not exceed 60 percentile points.
- Isolated wet = precipitation exceeds the 80th percentile and previous timestep precipitation was less than 80th percentile & change from previous timestep did not exceed 60 percentile points.
- Recurring dry (dry-to-dry) = precipitation is lower than 20th percentile & previous timestep precipitation was lower than 20th percentile.
- Recurring wet (wet-to-wet) = precipitation is higher than 80th percentile & previous timestep precipitation was higher than 80th percentile.
- Dry-to-wet whiplash (dry-to-wet) = precipitation percentile increased by at least 60 percentile points from previous timestep.
- Wet-to-dry whiplash (wet-to-dry) = precipitation percentile decreased by at least 60 percentile points from previous timestep.

In this case, a timestep refers to either a year (for annual analysis) or a season (for seasonal analysis). Seasons were defined as winter (December-February), spring (March-May), summer (June-August), and fall (September-November). For a given location, percentiles were calculated based on the entire historical period for that timestep (i.e., the percentile for summer 2023 at a grid cell was calculated based on summer precipitation from all years at that grid cell). Seasonal extreme identification was then based on sequential timesteps (i.e., summer 2023 at a grid cell was classified into one of the six typologies above based on the summer 2023 percentile and the spring 2023 percentile).

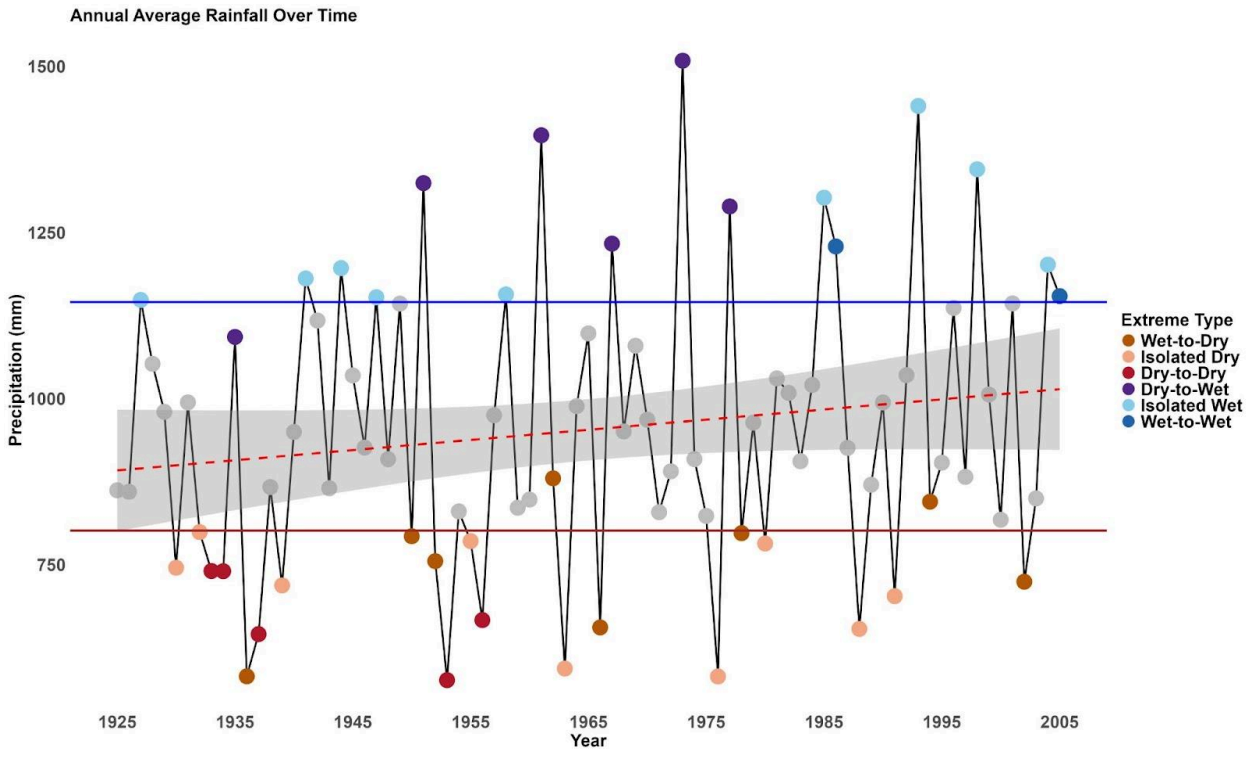

Figure 1. Illustration of the classification of annual precipitation extremes from time series data. Points are colored according to extreme event type, defined by percentile thresholds and year-to-year changes as described in the text: isolated wet and dry years (above 80th and below 20th percentiles), recurring extremes (two or more consecutive years of wet or dry), and whiplash transitions (rapid shifts from wet-to-dry or dry-to-wet). Horizontal lines show the 80th (blue) and 20th (brown) percentile thresholds used for classification. Data shown here uses annual precipitation at the PRISM grid cell nearest to the USGS streamflow gauge 06892350 (Kansas River near De Soto).

1.2 Data source evaluation and database development

We compiled daily station-based precipitation data from the NOAA Global Historical Climatology Network-Daily (GHCN-D) and monthly gridded meteorological data from the Parameter-elevation Regressions on Independent Slopes Model (PRISM) dataset. PRISM data have the advantage of being spatially and temporally continuous, but gridded datasets often show reduced skill in representing the magnitude and timing of daily extreme events, especially for cold extremes and heavy precipitation (Smith et al., 2025). To evaluate the accuracy of historic PRISM data for extreme identification at seasonal to annual timescales, we compared PRISM data to long-term meteorological stations across the Great Plains region. The larger U.S. Great Plains region was selected for this comparison to increase the sample size of GHCN-D stations relative to Kansas alone. We found that for our seasonal to annual analysis, PRISM generally had strong agreement for both total precipitation and extreme identification when compared to

station-based data (slopes near 1 and $R^2 > 0.9$ for comparisons of station-based and PRISM total precipitation and extreme counts). Seasonal comparisons reveal the highest correlations in spring and fall, while winter months (especially January and February) exhibit greater variability, consistent with challenges in representing snowfall and frozen precipitation. Overall, this comparison affirmed PRISM's suitability for analyzing spatiotemporal variability in seasonal to annual extremes in the Great Plains region. This analysis updates and extends previous work reported in Preota et al., 2025. Full details are described in this section and Appendix 1.

1.2.1 Data curation

To ensure completeness and reliability of historical station-based precipitation data, we implemented a systematic data curation process that involved using nearby stations and long-term PRISM data to fill gaps when necessary. Note that the station data curation and PRISM validation comparisons (Section 1.2) use data from 1900 to June 2024, as many stations lacked observations prior to 1900. The subsequent analysis of precipitation extremes in Sections 2 and 3 uses 1895–2023 for consistency with the full PRISM record. For curation, the initial station dataset contained 538 stations within the Great Plains region, from which stations with less than 10% missing data were selected (n = 234). The percentage of missing data for each station was calculated based on the total number of missing data points divided by the total number of possible days in the dataset. To address missing values, we employed a three-step imputation strategy:

Step 1: Station-Based Daily Gap-Filling. For each station with missing data, we identified nearby stations within a 45 km radius and calculated the correlation coefficient (R^2) between their daily precipitation records. The 45 km distance threshold was selected based on a balance between spatial proximity and data availability. We aimed to include a sufficient number of nearby stations to ensure meaningful correlation analysis (R^2) while maintaining geographic relevance. Then the most correlated station ($R^2 > 0.5$) was used to fill gaps in daily station data. If no nearby stations met this criterion, or nearby stations had missing data on the same date, the missing daily data remained unfilled. From these, 140 stations had at least one nearby station within a 45 km radius. Filtering based on $R^2 > 0.5$ reduced the number of eligible stations to 123.

Step 2: Aggregation to Monthly Totals. Because this project focuses on seasonal-to-annual hydroclimatic extremes, daily precipitation data were aggregated into monthly totals after station-based daily gap-filling.

Step 3: PRISM-Based Monthly Gap-Filling. If more than 10% of the daily data for a given station and month remained missing after daily gap-filling interpolation, we replaced the station-based monthly total with PRISM monthly precipitation data from the nearest PRISM grid point. To assess the extent of gap-filling, we calculated the total number of monthly data points across all stations (363,636 total months from 234 stations) and the number of months where PRISM was used to replace missing station data (25,091) from 1895 to June 2024, which accounts for 6.9% of the total dataset.

Following these curation steps, we had a gapless monthly precipitation dataset for each station. We then used this precipitation dataset to calculate seasonal and annual precipitation totals and precipitation extremes following the approach described in Section 1.1.

1.2.2 Comparison of station-based and PRISM precipitation

Because PRISM data is derived from station-based precipitation, we anticipated a strong agreement between the two datasets. However, due to the smoothing inherent in gridded datasets, we compared them to assess whether systematic issues with PRISM data made it unsuitable for our analysis (i.e., underestimation of extremes) and identify potentially anomalous station values (i.e., due to sensor issues).

Annual precipitation comparison: To assess agreement between station and PRISM data, we conducted linear regression analyses comparing station-measured total annual precipitation with PRISM-derived precipitation. Figure 2 presents the distribution of slope, R^2, and intercept values from yearly regression models while Figure 3 shows these metrics for monthly models. The slopes, mostly centered around 1.0, indicate a strong agreement between PRISM and station-based precipitation. The R^2 values predominantly exceed 0.9, indicating good agreement between PRISM and station data for annual precipitation.

Seasonal precipitation comparison: To further evaluate seasonal variability, we performed monthly regression analyses (Figures 3–5). Results showed that PRISM consistently captured station precipitation patterns across months with a similar degree of agreement as annual data, showing most R^2 values exceeding 0.9 and most slopes close to 1.0 (Figure 3). However, there were seasonal differences in the agreement between stations and PRISM, with the highest correlations ($R^2 > 0.9$) observed in April and October. In contrast, lower correlations (<0.6) occurred in winter months (December-February), likely due to differences in precipitation phase (rain vs. snow), measurement inconsistencies, or spatial interpolation limitations in PRISM data.

Evaluating Anomalies and Outliers: Among the 234 stations, 15 had at least one month where PRISM estimates exhibited an $R^2 < 0.5$ compared to station records. Figure A2 highlights these months, showing that discrepancies were most common in winter months. To investigate further, we plotted total monthly precipitation from station records against PRISM-derived values for cases where $R^2 < 0.5$ (Figure A2). An example anomaly is the case of station USC00410120 (Albany, Texas) in March 2004, where PRISM estimated 451 mm of precipitation—far exceeding the official station record of 33 mm for the entire month. Historical records indicate that a severe weather event occurred on March 4, 2004, involving tornadoes and large hail, yet the observed station precipitation depth remained low (Overpeck et al., 2010). Given the number of anomalous months in the full dataset was small and it was unclear when the differences were due to issues with station data as opposed to PRISM data, we elected to use PRISM data for subsequent analytical steps.

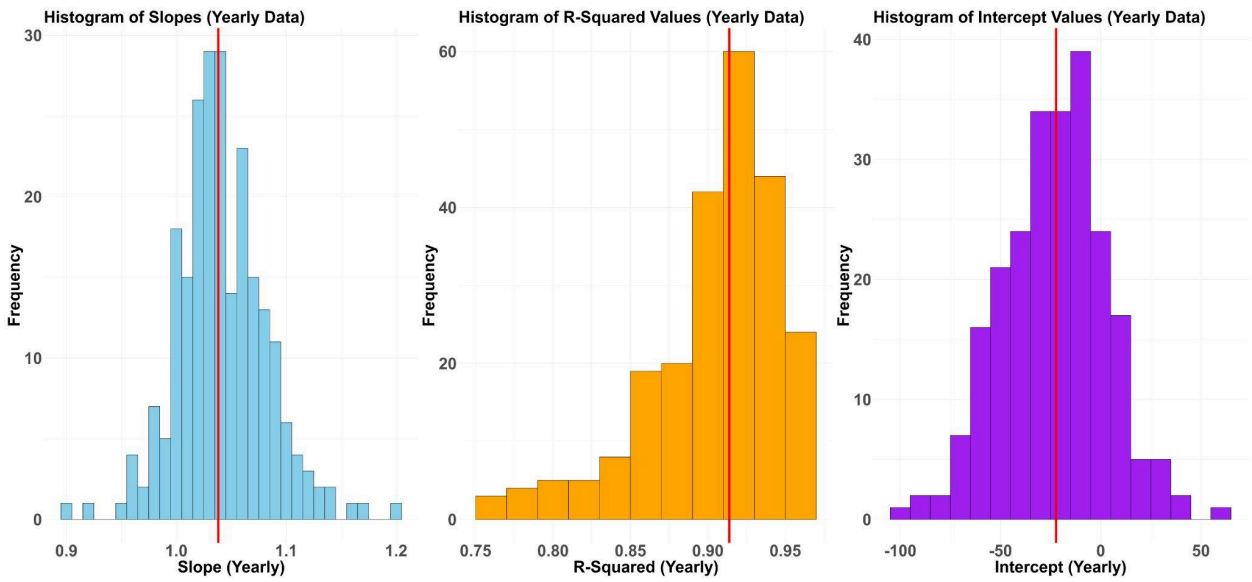

Figure 2. Histograms showing the distribution of slopes (left), R^2 values (center), and intercept values (right) for yearly precipitation data between station observations and PRISM data. In the regression model used for this analysis, the station-measured total precipitation is the dependent (y) variable while the PRISM-derived total precipitation is the independent (x) variable. The red vertical line shows the median for each plot.

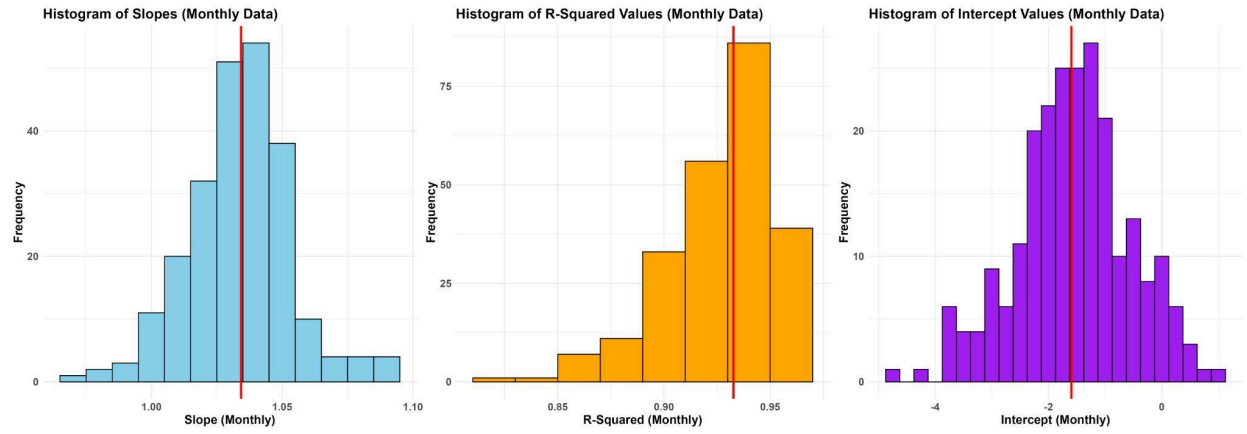

Figure 3. Histograms showing the distribution of slopes (left), R^2 values (center), and intercept values (right) from station-PRISM regression models for monthly precipitation data. In each case, the station-measured total precipitation is the dependent variable (y) and PRISM-derived precipitation is the independent variable (x). The red vertical line shows the median for each plot.

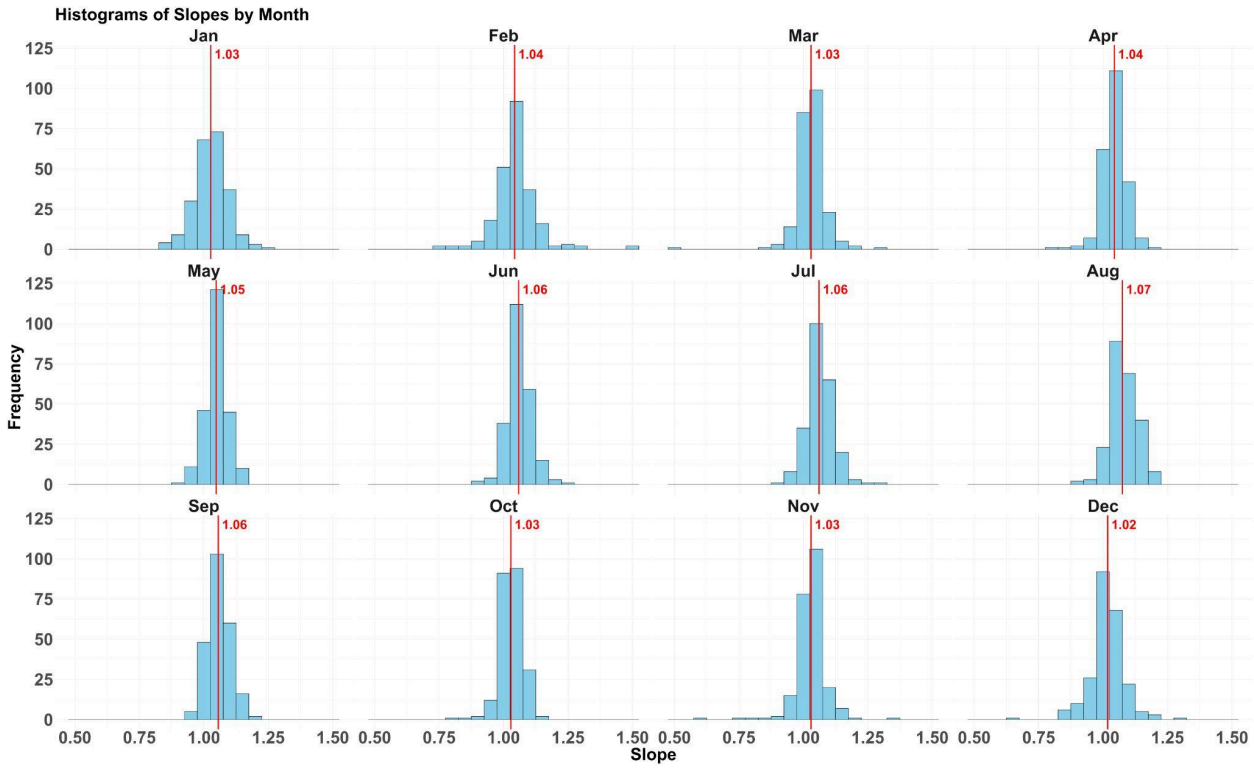

Figure 4. Histograms of monthly slope values comparing station observations and PRISM data. In the regression model used for this analysis, the station-measured total precipitation is the dependent (y) variable while the PRISM-derived total precipitation is the independent (x) variable. Each panel represents a different month, showing the distribution of slopes from the linear regression models. The red vertical line shows the median for each plot, which is labeled with the median R^2 value.

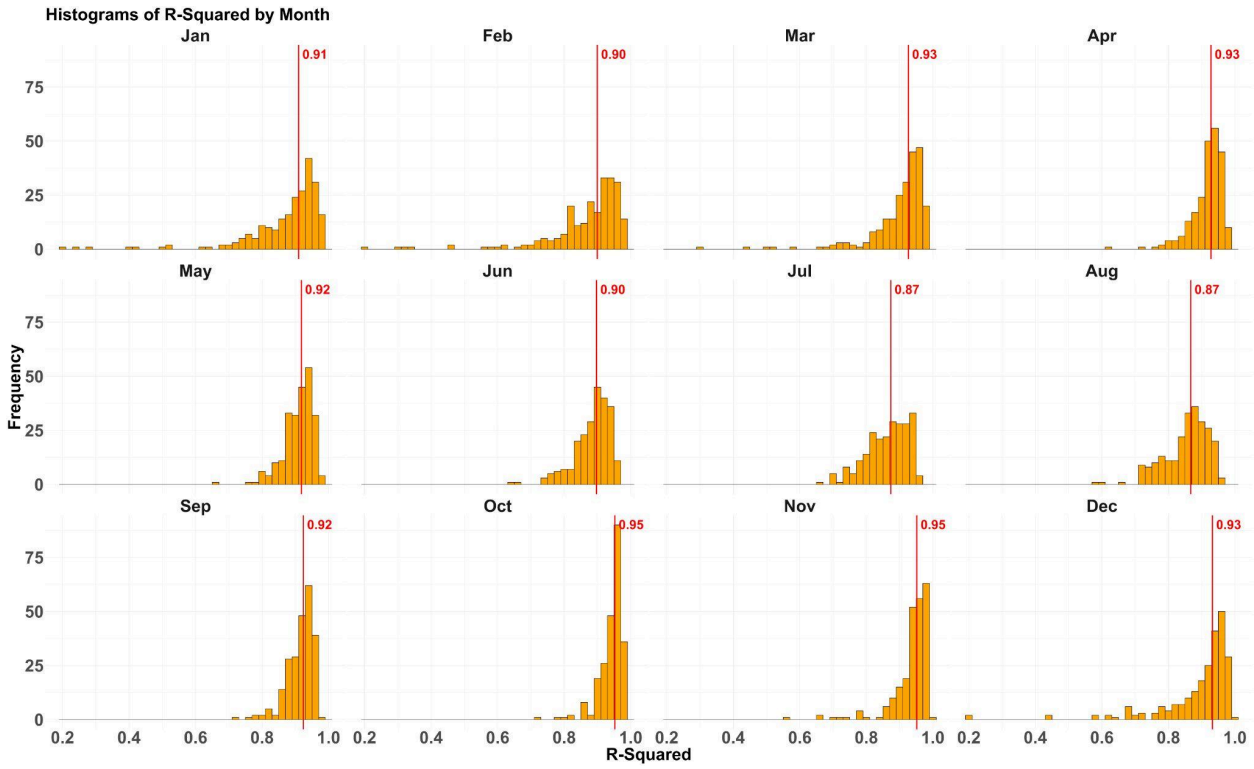

Figure 5. Histograms of monthly R^2 values between station observations and PRISM data for 1900–2023, demonstrating seasonal variations in correlation strength. In the regression model used for this analysis, the station-measured total precipitation is the dependent (y) variable while the PRISM-derived total precipitation is the independent (x) variable. Months like April and October show the highest correlations, with most R^2 values exceeding 0.9. The red vertical line shows the median for each plot, which is labeled with the median R^2 value.

1.2.3 Comparison of station-based and PRISM extremes

To evaluate potential differences in extreme identification between station-based and PRISM data, we conducted a comparative analysis of annual and seasonal extreme counts (Figures 8–12). These extreme categories were quantified separately for both PRISM and station annual data (1895–2023), and the PRISM cell closest to each station was extracted for comparison to evaluate agreement using density heatmaps (e.g., Figure 8) and fit statistics (e.g., Table 1).

Annual extreme comparison: The annual comparison reveals a strong overall correlation between PRISM and station-based extreme counts, though systematic differences exist (Figure A3). Dry extremes exhibit the highest deviation (mean absolute error [MAE] = 1.66 extremes, Table 1), suggesting that PRISM and station data diverge the most for these types of extremes. Whiplash extremes (dry-to-wet, wet-to-dry) and normal conditions show moderate discrepancies, while recurring wet events (wet-to-wet) have the lowest MAE (1.18 extremes), indicating better agreement between the two datasets. Figure 6 illustrates the percent bias (PBIAS) between

PRISM and station-based extreme event counts across six annual extreme types, showing that PRISM tends to overestimate dry and dry-to-wet events while underestimating dry-to-dry and wet extremes, highlighting subtle biases in capturing transitions between hydroclimatic states.

Seasonal extreme comparison: Seasonal variations are examined in Figures 9–12 and Table 1, which further explore the distribution of extreme event counts in winter, spring, summer, and fall from March 1895 to May 2024:

- The winter comparison (Figure A4) shows a generally positive correlation between PRISM and station-based extreme counts across all types of extremes. However, deviations from the 1:1 line indicate differences, with station observations often recording fewer extreme events than PRISM. Error metrics (Table 1) further quantify these differences, with dry events exhibiting the highest MAE (1.67 extremes), suggesting greater disagreement between PRISM and station data for these extremes. Conversely, wet-to-wet events show the lowest MAE (1.08 extremes), indicating better agreement. Whiplash events (dry-to-wet, wet-to-dry) and wet extremes also show moderate discrepancies, highlighting variations in how extreme events are captured across datasets.
- The spring comparison (Figure A5) shows a strong correlation between PRISM and station-based extreme event counts across all event types, with some deviations from the 1:1 line, indicating differences in how extreme events are captured. Error metrics (Table 1) reveal that dry events have the highest MAE (1.65 extremes), suggesting greater discrepancies between PRISM and station data for these extremes. Conversely, wet-to-wet events exhibit the lowest MAE (1.22 extremes), indicating better agreement.
- The summer comparison (Figure A6) shows a strong correlation between PRISM and station-based extreme event counts, with deviations from the 1:1 line indicating differences in how extreme events are recorded across datasets. Error metrics (Table 1) reveal that wet and dry extremes exhibit the highest MAE values (both at 1.56 extremes), suggesting greater discrepancies between PRISM and station data for these extremes. Whiplash extremes (dry-to-wet, wet-to-dry) also show moderate errors, while dry-to-dry and wet-to-wet extremes have the lowest MAE (1.11 and 1.16 extremes, respectively), indicating better agreement between the two datasets for recurring extremes.
- Similarly, the fall comparison (Figure A7) shows a strong correlation between PRISM and station-based extreme counts, though deviations from the 1:1 line indicate differences in capturing extremes. Error metrics (Table 1) reveal that dry events exhibit the highest MAE (1.68 extremes), suggesting greater discrepancies between PRISM and station data for these extremes. Wet-to-dry events also show notable differences (MAE = 1.60 extremes), while wet-to-wet events have the lowest MAE (1.03 extremes).

Figure 7 shows the seasonal percent bias (PBIAS) between PRISM and station-derived extreme event counts, revealing that PRISM tends to underestimate dry-to-dry and wet-to-wet events in spring and fall, respectively. Inspection of selected extreme time series provided some clues as to potential causes for differences between PRISM and station-based extreme event counts. These include PRISM's interpolation process, which smooths spatial variability (Daly et al., 2008) and may result in less pronounced year-to-year fluctuations compared to individual station records (indicated by the median slope exceeding 1 in Figure 3). Unlike a single station's dataset, which captures localized peaks and troughs, PRISM aggregates data over a broader spatial scale, potentially reducing the intensity of extremes through spatial averaging and interpolation. Because PRISM relies on meteorological station data as the basis for its interpolation, it may be more accurate at the station locations relative to areas between stations. Additionally, small variations in precipitation values can shift percentile classifications, leading to differences in extreme event identification between the two datasets even when actual precipitation values are similar. However, the percent bias is small overall, with a maximum absolute value of approximately 5% at the annual timescale (Figure 6) and 10% at the seasonal timescale (Figure 7), with most extremes having less than 2% bias.

Table 1. Mean Absolute Error (MAE) for station vs. PRISM extreme counts across different extreme types. Timeline for analysis: annual (1895–2023) and seasonal (Summer 1895–Spring 2024). On average, station and PRISM-based extremes agree within 2 events for annual and all seasons.

Extreme Type	Annual	Winter	Spring	Summer	Fall
Isolated Dry	1.66	1.67	1.65	1.56	1.68
Dry-to-Dry	1.34	1.14	1.30	1.11	1.28
Dry-to-Wet	1.65	1.49	1.54	1.48	1.49
Isolated Wet	1.56	1.55	1.58	1.56	1.54
Wet-to-Dry	1.36	1.45	1.32	1.53	1.60
Wet-to-Wet	1.18	1.08	1.22	1.16	1.03

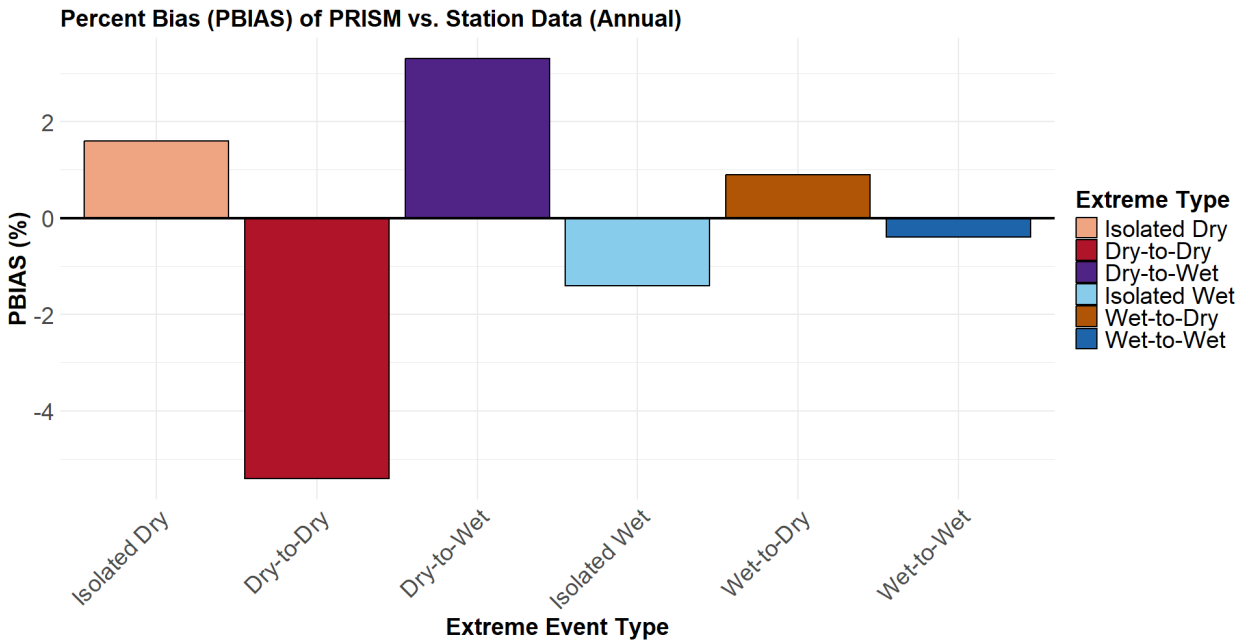

Figure 6. Bar plot showing the percent bias (PBIAS) between PRISM and station precipitation estimates across six extreme event types on an annual scale (1895–2023). PBIAS was calculated as the percent difference between PRISM- and station-derived counts for each extreme event type. Positive values indicate that PRISM detected more events than station data, while negative values indicate PRISM detected fewer events than station data.

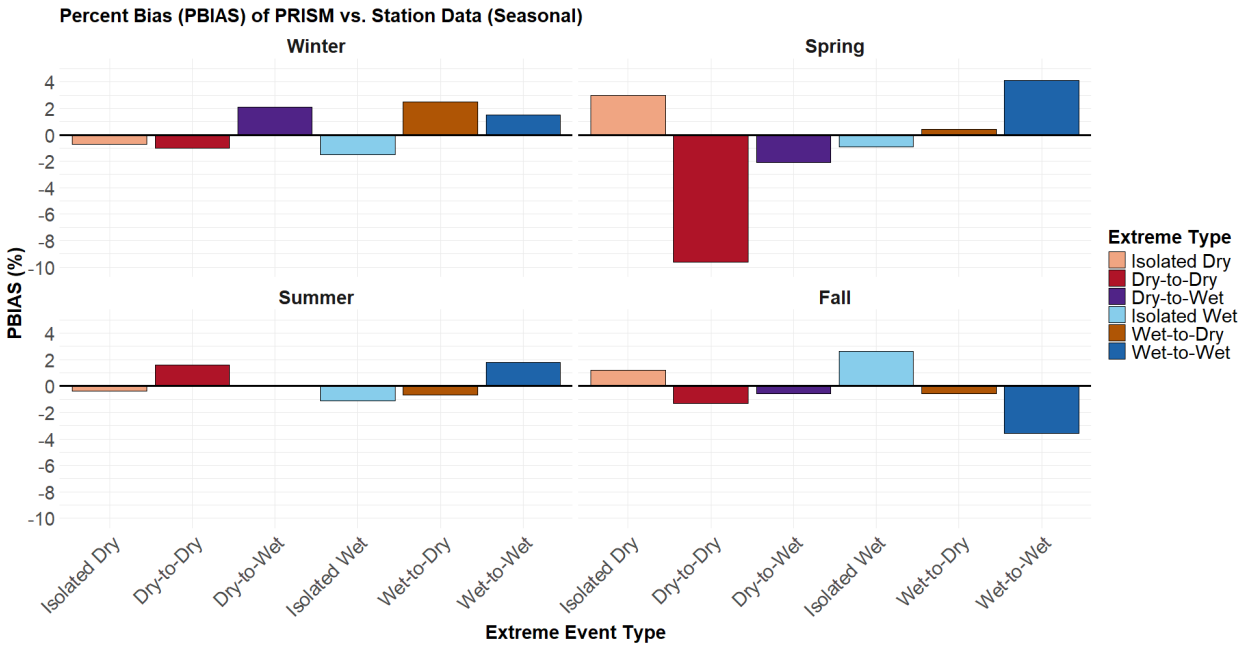

Figure 7. Comparison of percent bias (PBIAS) between extreme event counts derived from station observations and gridded PRISM data, disaggregated by season (Winter, Spring, Summer, Fall) for the period March 1895–May 2024. Each panel represents a different season, with bars indicating the percent difference between PRISM- and station-derived counts for six extreme event types. Positive PBIAS values indicate that PRISM identified more events than station data, while negative values indicate PRISM identified fewer events than station data.

1.2.4 Data comparison conclusions

Overall, we conclude that there is generally good agreement between PRISM- and station-based monthly and annual precipitation data. The median slope of a linear relationship between these two datasets is slightly above 1, indicating generally good agreement but a slight tendency for PRISM to underestimate during high precipitation years. The identification of seasonal to annual extremes and their classification into typologies was generally accurate, with MAE for the number of identified extremes between 1 and 2 for all extreme types and timescales over the 128-year period of annual comparison. This suggests that PRISM data are an appropriate tool for long-term analysis of seasonal to annual hydroclimatic extremes; they are the focus of subsequent analyses.

1.3 Data availability

We summarized annual and seasonal precipitation extremes for 148 water management areas across Kansas, including federal reservoir contributing areas (n = 24), groundwater management districts (GMDs; n = 5), Regional Advisory Committee (RAC) boundaries (n = 14), and counties (n = 105). For each area, the database includes precipitation totals and trends,

extreme type classifications, and decadal regime summaries as well as background information about land use/land cover conditions. These data are available through two channels:

- Interactive web tool (Objective 3): A map-based application allowing users to explore figures, narrative summaries, and downloadable spreadsheets for any management area.
- HydroShare: The full dataset of summarized figures and tables for the 148 management areas is available for download at http://www.hydroshare.org/resource/ec95b7fc57a54685b3aefe13a71c259e

For Objective 1, we used automated methods to compile and process these data for the broader U.S. Great Plains region to ensure that we had data for relevant upstream areas, such as watersheds of rivers that flow into the state, and to have a large sample of meteorological stations for comparison to PRISM. The summaries and analysis for Objectives 2 and 3 focus specifically on the state of Kansas, but the full regional database is available.

Objective 2: Analyze changes in hydroclimatic extremes in different water management areas.

2.1 Spatial and temporal patterns of precipitation change across Kansas

We observe an increasing annual precipitation trend across most of Kansas (Figure 8), which is significant (Mann-Kendall test, $p < 0.05$) over 40.3% of the state. Significant trends range from 4.32 to 14.72 mm/decade. The significant trend is strongest in the central and eastern portions of the state, including much of the Lower Arkansas River and Lower Republican River basins. There is also a significantly increasing annual precipitation trend in a pocket of west-central Kansas, corresponding to the Upper Smoky Hill River region and including much of Groundwater Management District 1 (GMD1). Seasonally, the increasing precipitation trend is predominantly driven by increases in spring precipitation (Figure 9), which are significant over 45.2% of the state. Similar to annual trends, the spring increases in precipitation are most common over the central and eastern portions of the state and range from 2.4 to 7.1 mm/decade.

Given Kansas's strong east-west precipitation gradient (Figure 8a), this indicates that the wettest portions of the state are receiving, on average, more annual rainfall. This finding is consistent with station-based analysis of Kansas's precipitation trends over the 1895–2015 period (Lin et al., 2017), though the precipitation trends in that study were not statistically significant. This may be due to the shorter time period of analysis or lumping of multiple stations into regions in Lin et al., 2017, which may mix areas with significant and non-significant trends (Figure 8b) and produce a non-significant overall trend.

Despite the increasing precipitation trends we observe, it is possible that the state may be experiencing drier overall conditions. Our study did not analyze changes in evapotranspiration (ET), but other work has shown that increases in potential ET exceed changes in precipitation and are leading to overall drier conditions across the U.S. Great Plains region (Seager et al., 2017).

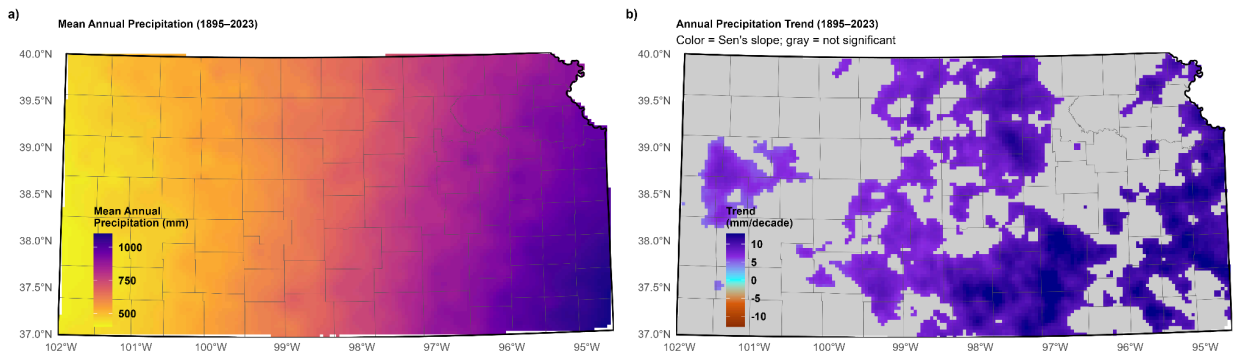

Figure 8. (a) Map showing the mean annual precipitation of Kansas and (b) map showing long-term trend (Sen's slope, mm/decade), both for the 1895–2023 period. On (b), locations with non-significant trends are colored gray.

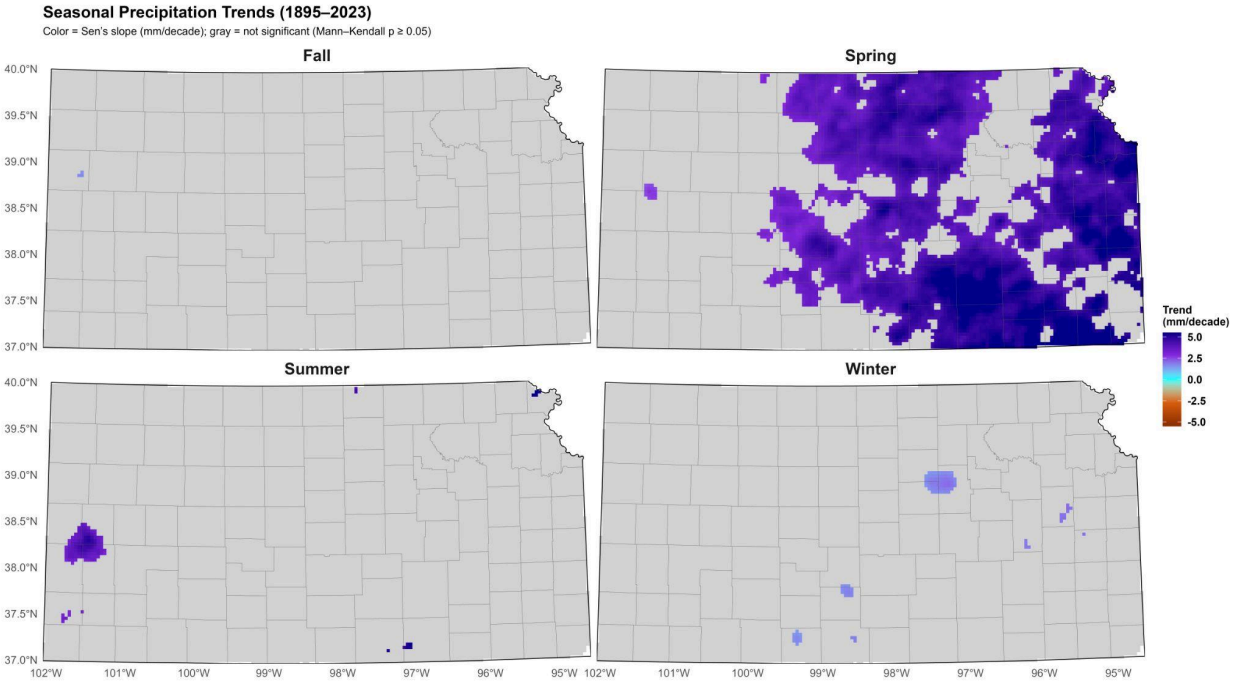

Figure 9. Seasonal precipitation trend maps for Kansas for the 1895–2023 period. Locations with non-significant trends are colored gray.

2.2 Temporal changes in precipitation extremes across Kansas

Kansas's precipitation is highly variable, and we observe that each of the extreme types we identified occurs in Kansas throughout the entire period of record. At the annual scale, two extreme types (isolated wet and recurring wet-to-wet) have significantly increasing linear trends, indicating that these types of extremes have become, on average, more widespread in Kansas from 1895 to 2023 (Figure 10). Wet-to-wet extremes, in particular, have become substantially more common, with very infrequent occurrences prior to 1980 and presence in at least part of the state almost every year since 1980. Other types of extremes do not have significant linear trends but do exhibit notable changes in extent through time. Isolated dry and dry-to-dry extremes had the greatest overall extent in the first half of the period of record, with notable spikes in the 1910s and well-known droughts such as the Dust Bowl of the 1930s and the state's drought of record in the 1950s. Whiplash type (dry-to-wet and wet-to-dry) extremes tended to occur more evenly throughout the entire period of record, though they appear to have a lower average spatial extent over the past three decades. These patterns are similarly true when we summarize to wet-type and dry-type extreme occurrences by decade as we observe dry-type extremes most common in the 1910s, 1930s, and 1950s, while wet-type extremes have been relatively common since the 1940s with an increase since the 1980s (Figure 11).

Seasonally, we observed that the average extent of isolated wet extremes was significantly increasing in winter and spring and wet-to-dry whiplash extent was significantly increasing in the summer (Figure 12). Because summer wet-to-dry is dependent on a shift from spring wet conditions to summer dry conditions, the increase in summer wet-to-dry may be primarily driven by an increase in spring precipitation (Figure 9) because there was not a significant trend toward dry conditions in the summer. While there were no significant trends for recurring extremes, we do observe that spring wet-to-wet conditions are visually more common since 1980 as well. In general, there are fewer clear temporal patterns for seasonal patterns than annual patterns, though we do observe more common dry-type extremes in the summer and fall during notable droughts in the 1930s and 1950s (Figure 13).

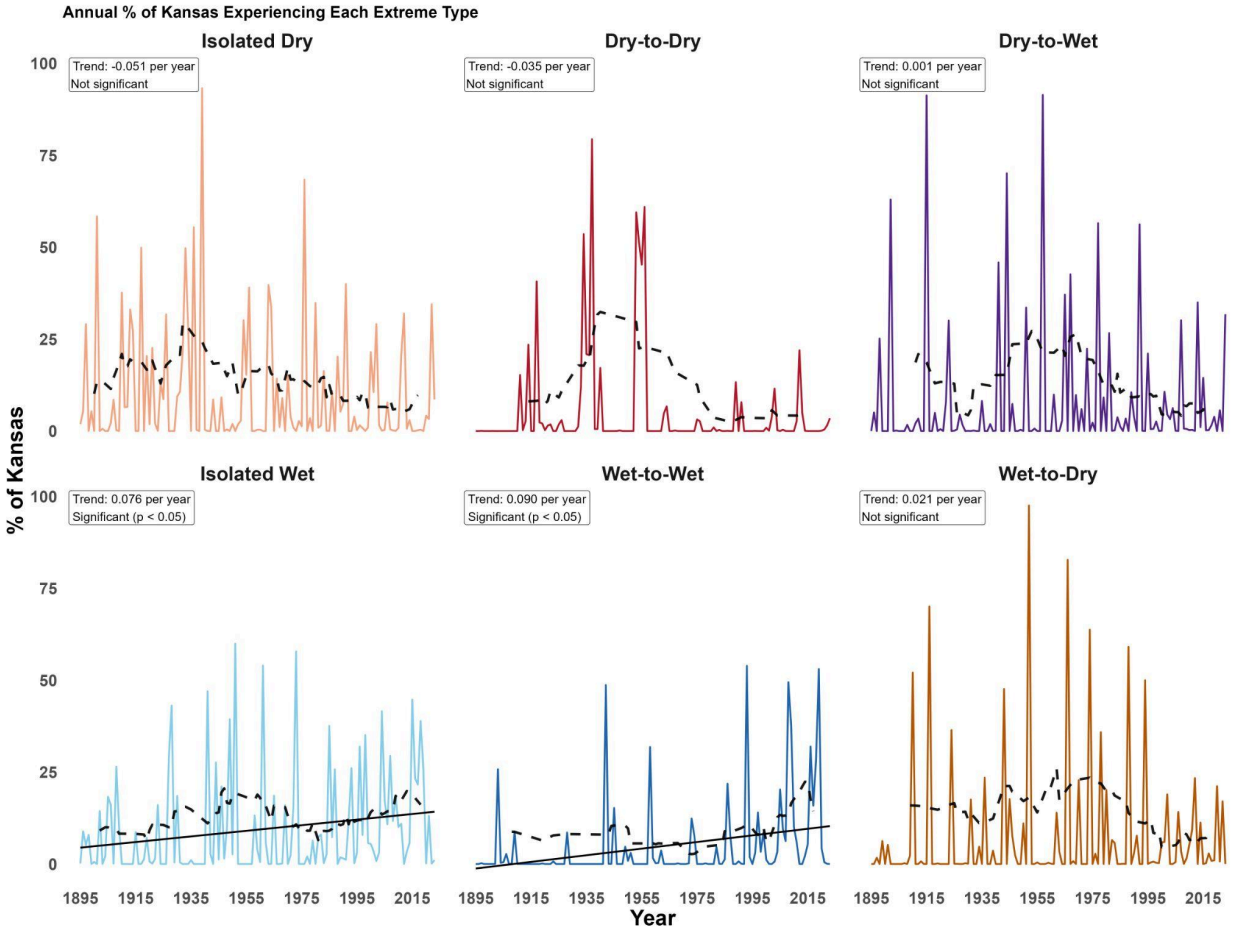

Figure 10. Annual percentage of Kansas experiencing each precipitation extreme type from 1895 to 2023. Panels display six categories: transitions between wet and dry years (Wet-to-Dry, Dry-to-Dry, Dry-to-Wet, Wet-to-Wet) and isolated extremes (Isolated Dry, Isolated Wet). Colored lines show annual values, black dashed lines indicate 9-year centered moving averages, and solid black lines denote significant long-term linear trends. The results highlight spatially aggregated frequencies of extremes across all grid cells, illustrating both year-to-year variability and directional changes over time.

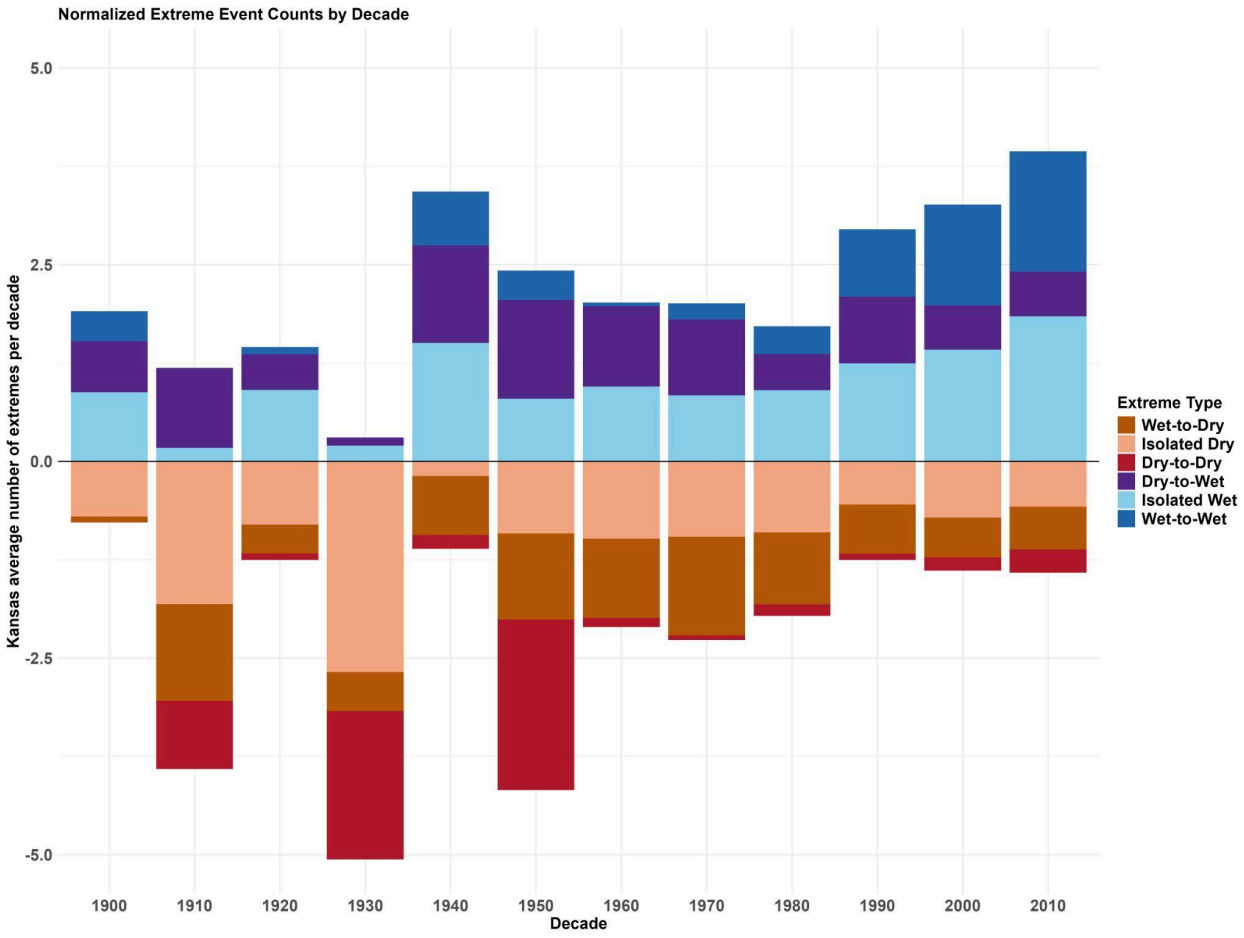

Figure 11. Average number of extremes per decade (1900–2020), grouped into wet-type (upward bars, positive count) and dry-type (downward bars, negative count) categories. The average number of extremes by decade is calculated by summing the total extreme-type occurrences across all PRISM grid cells within each decade and dividing by the total number of grid cells, yielding the mean number of extreme years per location per decade.

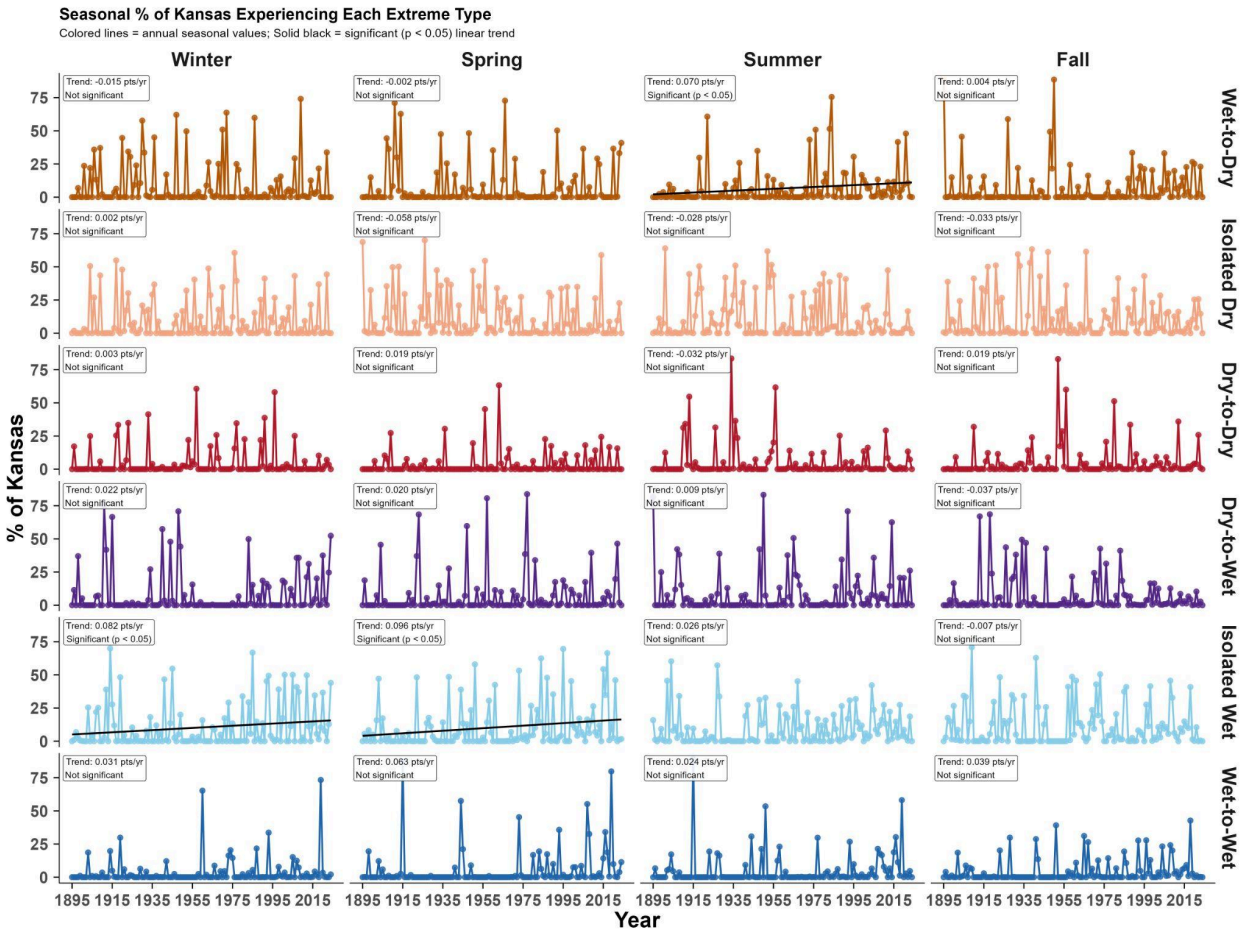

Figure 12. Percentage of Kansas experiencing each seasonal precipitation extreme type from 1895 to 2023. Panels display six categories: transitions between wet and dry years (Wet-to-Dry, Dry-to-Dry, Dry-to-Wet, Wet-to-Wet) and isolated extremes (Isolated Dry, Isolated Wet). Colored lines show annual values and solid black lines denote significant long-term linear trends ($p < 0.05$). The results highlight spatially aggregated frequencies of extremes across all grid cells, illustrating both year-to-year variability and directional changes over time.

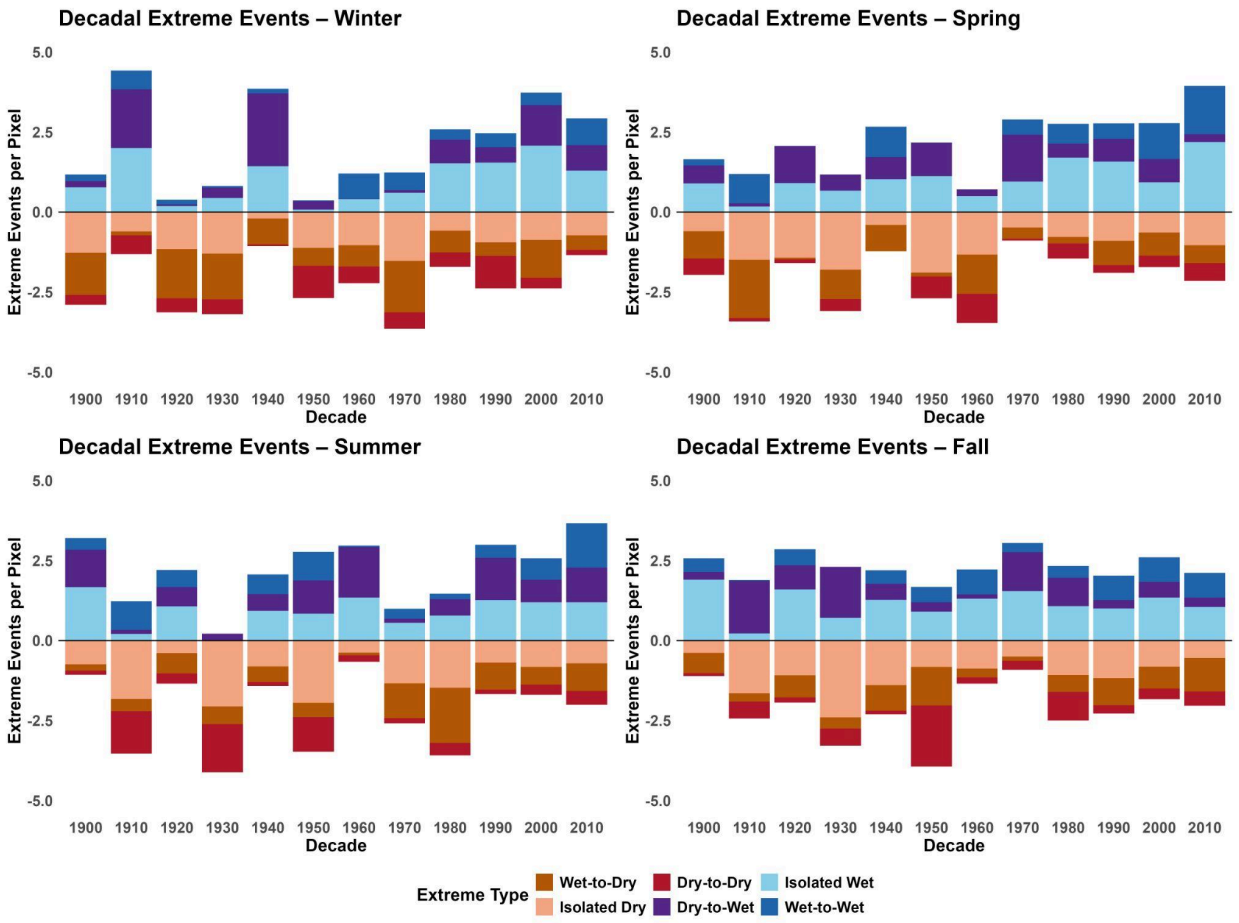

Figure 13. Average number of extremes per decade (1900–2020), grouped into wet-type (upward bars, positive count) and dry-type (downward bars, negative count) categories for each season. The average number of extremes by decade is calculated by summing the total seasonal extreme-type occurrences across all PRISM grid cells within each decade and season and dividing by the total number of grid cells, yielding the mean number of extreme seasons per location per decade for each season.

2.3 Spatial and temporal patterns of hydroclimatic extremes across reservoir contributing areas

2.3.1 Precipitation trend analysis

To assess seasonal to annual hydroclimate extremes for different management-relevant areas within the state, we focused on the 24 federally managed reservoirs in Kansas and summarized precipitation totals and extremes for all PRISM grid cells in their contributing areas (Figure 14). These watersheds span the state's strong east-west precipitation gradient, with watershed-average mean annual precipitation ranging from approximately 463 mm/yr in the west to over 1,000 mm/yr in the east, and extend into Nebraska to the north and Colorado to the west. Long-term trends were assessed using the Mann-Kendall trends and Sen's slope estimator (as in Section 2.1); all 24 reservoirs exhibited positive annual precipitation trends within their watersheds ranging from 3.1 to 12.7 mm/decade. The increasing annual precipitation trend was

statistically significant ($p < 0.05$) for 8 reservoirs. The strongest increasing trends were concentrated in southeastern catchments such as El Dorado and Fall River, which are the wettest parts of the state, though we also observed significant increasing annual precipitation trends at central reservoirs (Cheney, Waconda, Lovewell, Milford) and Cedar Bluff Reservoir, which has the westernmost and driest watershed of any federal reservoir in the state. These increasing precipitation trends may be partially or fully counteracted by historical changes in ET, which were not assessed in our analysis.

Seasonally, the increasing annual precipitation trends in reservoir watersheds are predominantly driven by increasing precipitation in the spring (March-May), consistent with the statewide patterns observed in Figure 8. Spring precipitation trends were positive across all 24 reservoirs (Figure 15), ranging from 1.6 to 5.4 mm/decade, with 17 of 24 showing statistically significant increases ($p < 0.05$; Figure 15). The strongest spring trends were concentrated in southeastern catchments such as Elk City (5.4 mm/decade), El Dorado (4.9 mm/decade), and Fall River (4.9 mm/decade), with significant increases also observed at central reservoirs including Milford (4.4 mm/decade) and Tuttle Creek (4.4 mm/decade). No reservoir exhibited a statistically significant trend in any other season. Winter trends were uniformly positive but small (0.1–1.6 mm/decade), summer trends ranged from −0.5 to 3.4 mm/decade, and fall trends spanned −1.0 to 1.8 mm/decade — all non-significant.

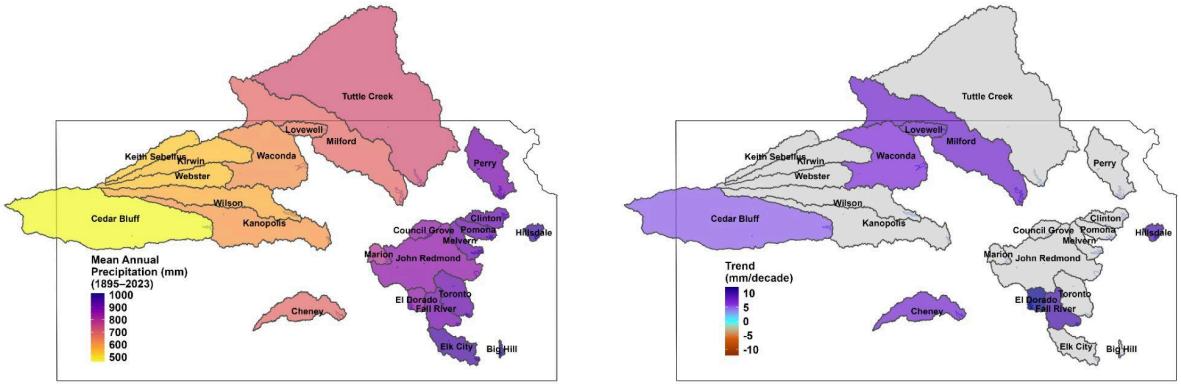

Figure 14. Mean annual precipitation (1895–2023) and long-term precipitation trends across Kansas reservoir catchments. (a) Mean annual precipitation (mm) by catchment, showing a clear west-to-east gradient of increasing precipitation across the state. (b) Sen's slope of annual precipitation trends (mm/decade); gray catchments indicate non-significant trends ($p \geq 0.05$).

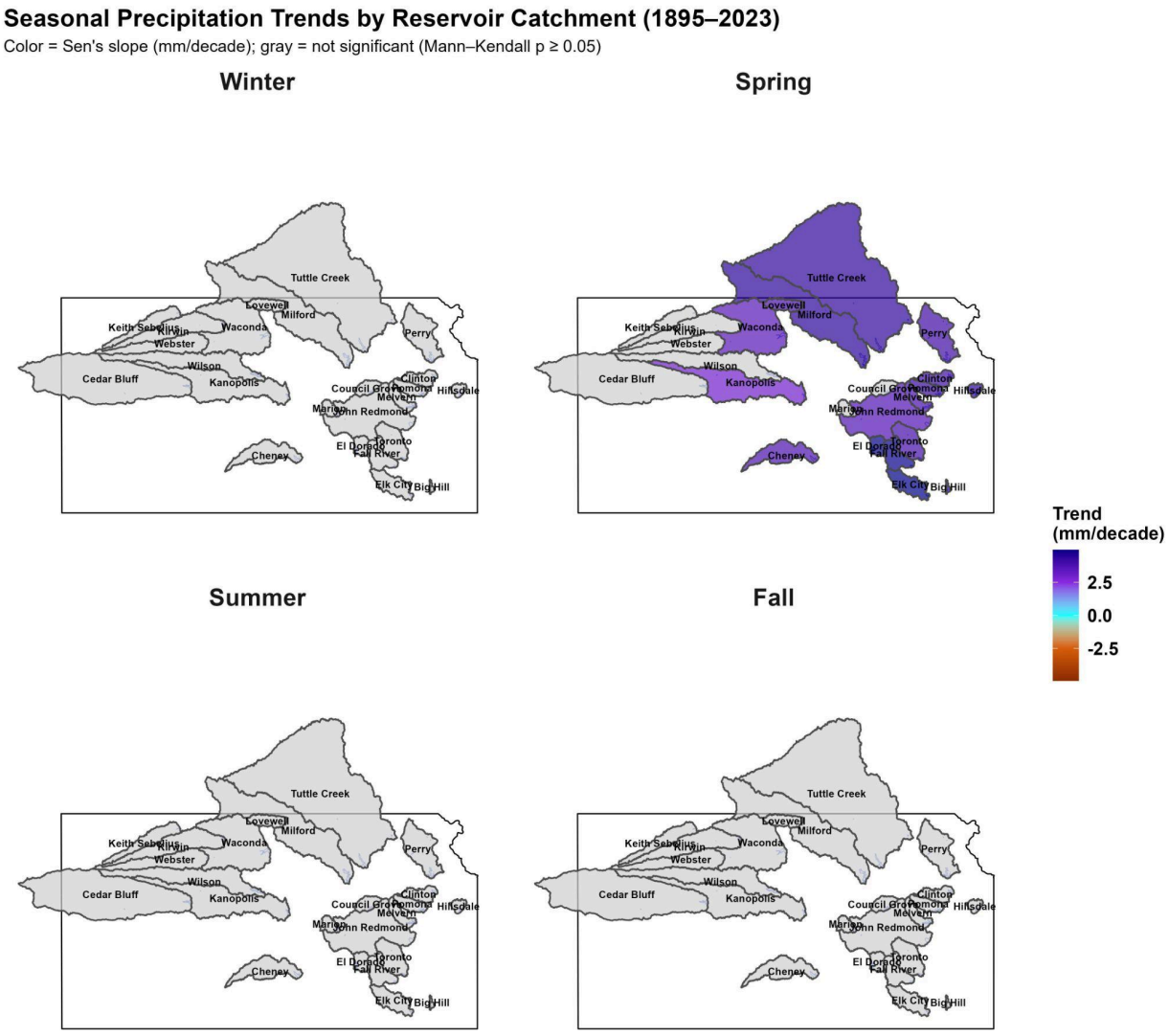

Figure 15. Seasonal precipitation trends across Kansas reservoir catchments (1895–2023) for winter, spring, summer, and fall. Color indicates Sen's slope of seasonal total precipitation (mm/decade); gray catchments indicate non-significant trends (Mann-Kendall $p \geq 0.05$).

2.3.2 Spatial patterns of extremes

We used the annual and seasonal watershed-average precipitation for each reservoir to then identify historical extremes following the percentile-based extreme typology described in Section 1.1. We also developed two derived metrics — the wet-dry index and the whiplash ratio — to investigate spatial patterns in precipitation extremes, focusing on the most recent 40-year period (1984–2023).

The wet-dry index was constructed by assigning each extreme type a score reflecting its position on the wet-dry spectrum (isolated wet = +1, wet-to-wet = +2, dry-to-wet = +1, wet-to-dry = −1, isolated dry = −1, dry-to-dry = −2) relative to a neutral baseline (normal

conditions = 0) and averaging these scores across the 1984–2023 period. At the annual scale, the wet-dry index is positive across all reservoirs, though its magnitude varies considerably across the state, ranging from 0.12 at Cedar Bluff to 0.35 at Cheney (Figure 16). In general, the higher wet-dry index values are for central and eastern reservoirs such as Cheney, El Dorado, Milford, and Fall River, indicating these reservoirs are disproportionately exposed to annual wet extremes.

Seasonally, the wet-dry index has the greatest positive values in the spring (mean wet-dry index = 0.146), followed by winter (0.092), summer (0.079), and fall (0.017) (Figure 17). This indicates that wet precipitation extremes have most strongly outnumbered dry extremes in the spring in recent decades. However, the spatial patterns differ among seasons. In spring, Cheney reservoir has the strongest wet-dry index, followed by Tuttle Creek, while in the winter Milford and Elk City have the strongest positive index values. Negative fall wet-dry indices are present in portions of the central and northeastern sections of the state, including Kanopolis, Cheney, Council Grove, and John Redmond reservoirs, indicating that wet extremes are less common than dry extremes over the past 40 years during the fall for these settings.

For the wet-dry index, the seasonal patterns do not directly add up to the annual value due to the approach for calculating this index. For example, Keith Sebelius has a positive annual wet-dry index (Figure 16) but negative and neutral seasonal wet-dry index values (Figure 17). The annual index is mainly driven by recurring wet years, which are more common than recurring dry years. Seasonally, however, conditions are much more variable — in particular, wet-to-dry whiplash events are concentrated in summer (7 of 40 seasons) and winter (4 of 40) for this reservoir, which causes those seasonal indices to be negative even though the full-year totals remain above average. As a result, the annual index appears wetter because cumulative moderate wetness across multiple seasons leads to a positive annual wet-dry index, but within-year whiplash leads to negative and neutral seasonal indices.

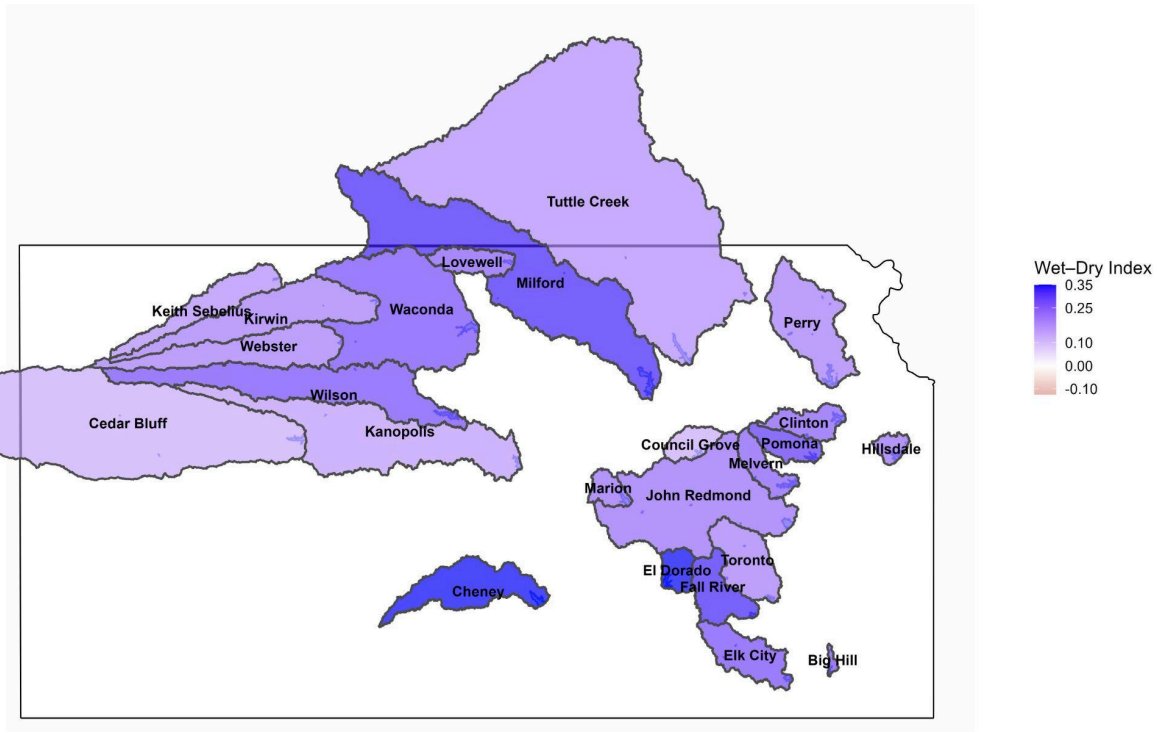

Figure 16. Annual wet-dry index across Kansas reservoir catchments (1984–2023). Positive values (purple) indicate a predominance of wet-type extreme years. All reservoirs have a positive annual wet-dry index, so there are no negative (red) values indicating a predominance of dry-type extremes.

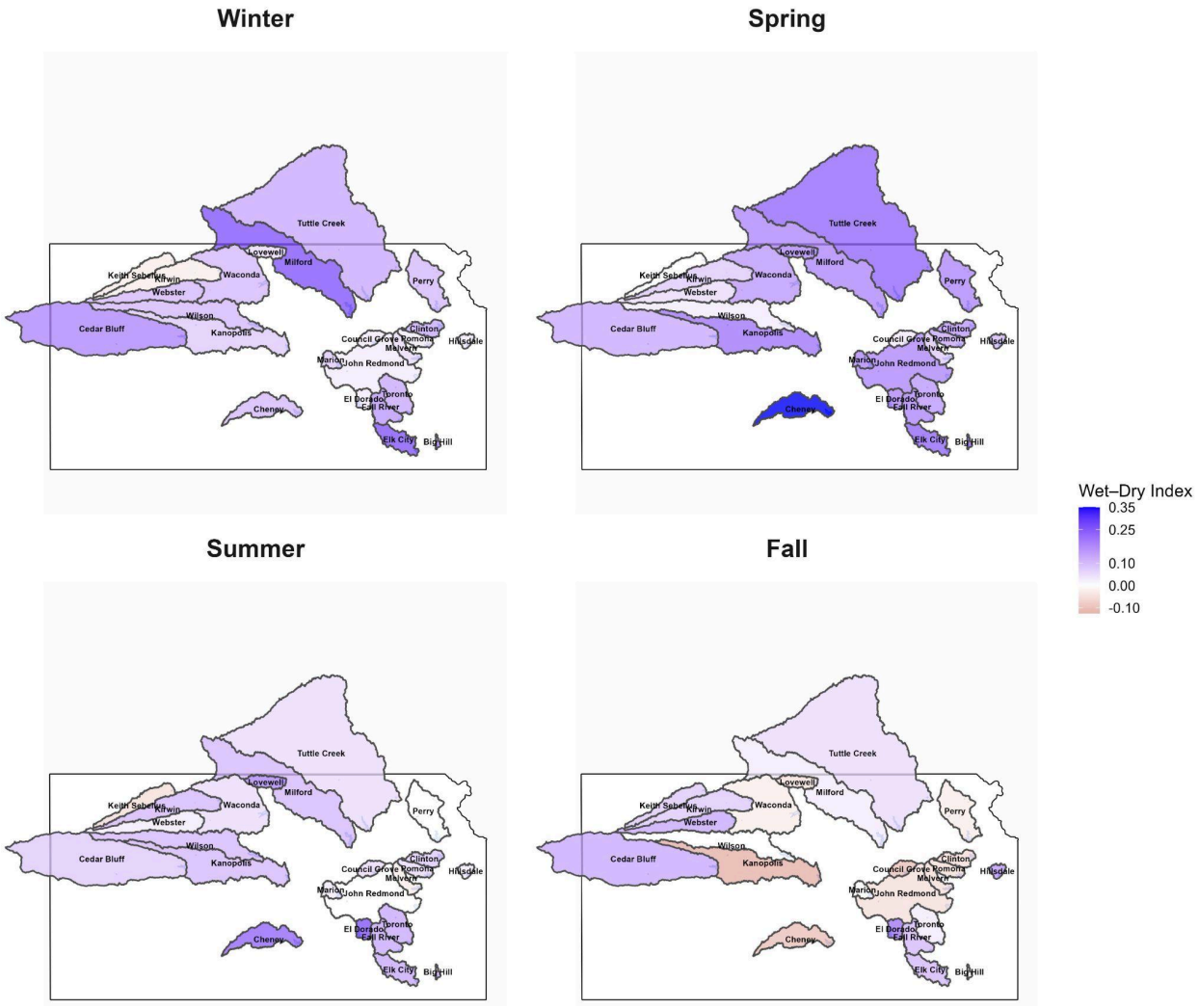

Figure 17. Seasonal wet-dry index across Kansas reservoir catchments (1984–2023) for winter, spring, summer, and fall.

The whiplash ratio captures the proportion of years (for annual assessment) or seasons (for seasonal assessment) in which a catchment experienced a rapid wet-to-dry or dry-to-wet transition, which we define as a shift of at least 60 percentile points between successive timesteps (see Section 1.1). Whiplash is most common in northern and eastern reservoirs at the annual scale (Figure 18). Of all reservoirs, the Marion Lake watershed had the highest whiplash ratio (0.20), indicating that 20% of years (or 1 in 5, on average) during 1984–2023 experienced rapid hydroclimatic transitions at this site. Seasonally, whiplash frequency is highest in summer (mean across all reservoir watersheds = 0.155; Figure 19), which is indicative of large wet-to-dry or dry-to-wet shifts between spring and summer seasons and makes sense given the large proportion of extremes that have occurred in the spring in the past 40 years (Figure 13). Because the high spring whiplash ratio is accompanied by a positive wet-dry index, this suggests that the majority of summer whiplash events are wet-to-dry, meaning a wetter-than-average spring

followed by a drier-than-average summer. After summer, whiplash is most common in the spring (mean whiplash ratio of 0.136, or whiplash occurring approximately once every 7 years), winter (mean whiplash ratio of 0.121, or whiplash occurring approximately once every 8 years), while fall shows the lowest frequency (0.103, or whiplash occurring approximately once every 10 years). Overall, this shows that seasonal wet-to-dry and dry-to-wet whiplash extremes are most common during the warm season across Kansas reservoir watersheds.

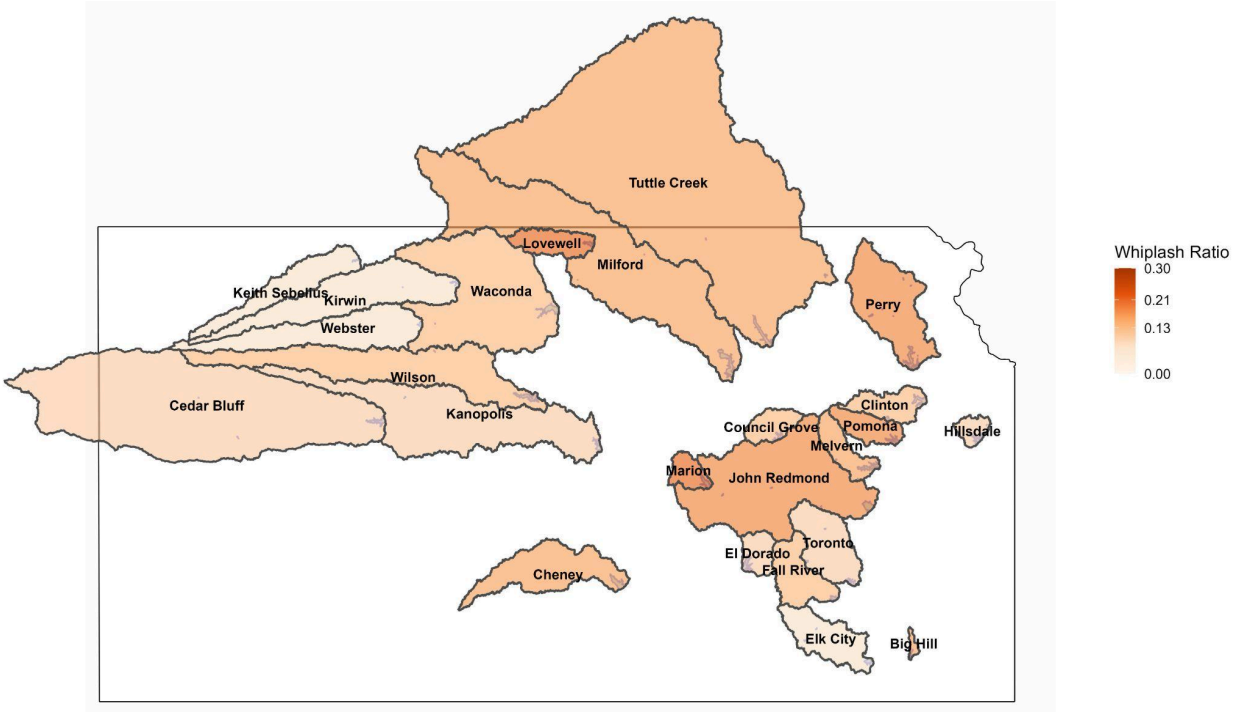

Figure 18. Annual whiplash ratio across Kansas reservoir catchments (1984–2023). The whiplash ratio represents the fraction of years experiencing abrupt wet-to-dry or dry-to-wet transitions relative to the total number of classified extreme years. Higher values (darker orange) indicate catchments with more frequent hydroclimatic reversals.

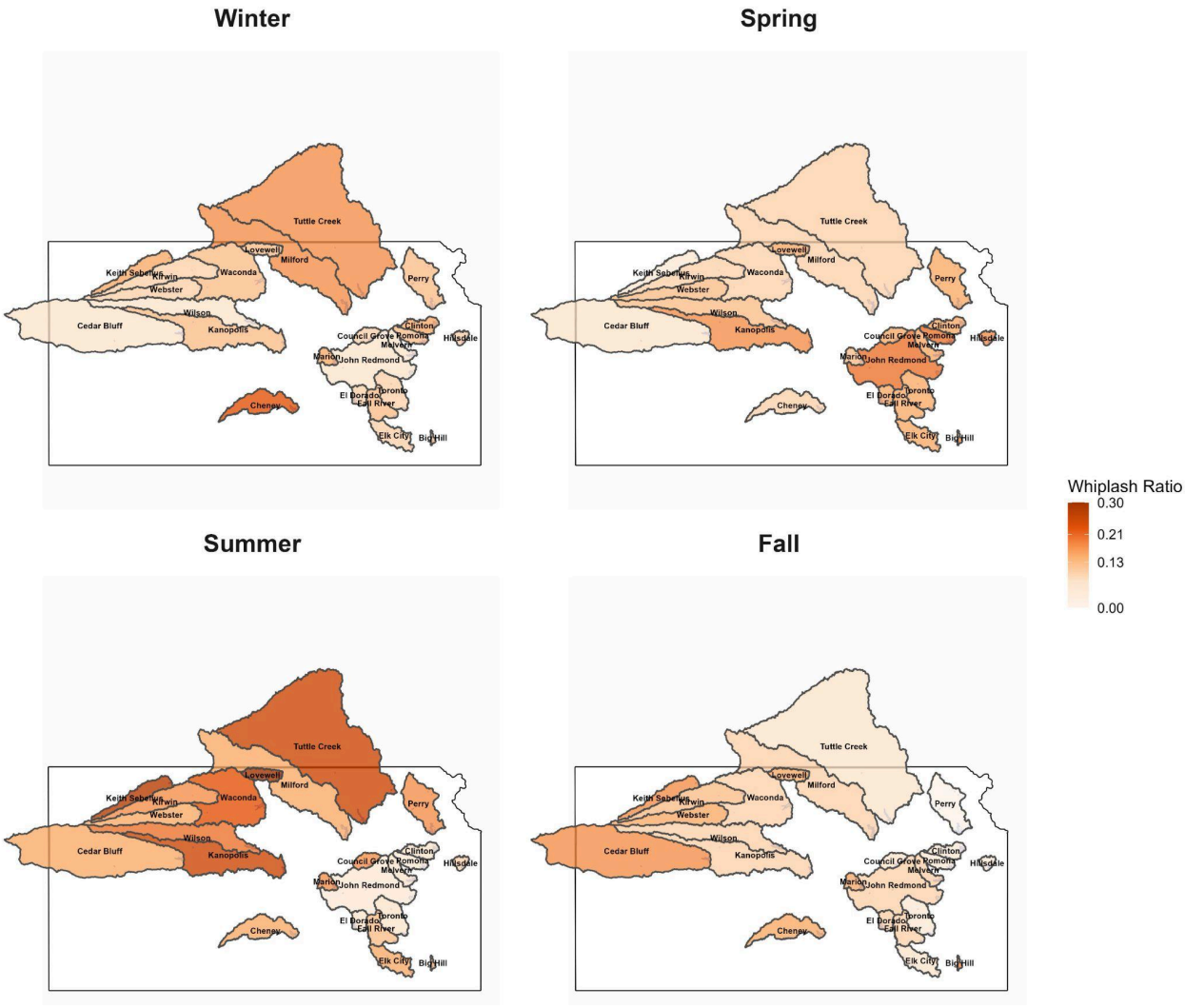

Figure 19. Seasonal whiplash ratio across Kansas reservoir catchments (1984–2023) for winter, spring, summer, and fall.

2.3.3 Annual and seasonal trends

Summarizing across all reservoirs, wet-type extremes (isolated wet, wet-to-wet, and dry-to-wet) are becoming significantly more frequent at the annual scale, while dry-type and total extreme counts show no significant trend (Figure 20a) — a pattern consistent with the statewide findings in Section 2.2. Seasonally, the only season and extreme type with a significant trend is an increased frequency of spring wet extremes (Figure 20b), mirroring the spring-dominated precipitation increase identified in Section 2.1 and reinforcing spring as the primary driver of the overall shift toward wetter conditions across Kansas reservoirs.

Spatially, significantly increasing wet extreme trends are concentrated primarily in central and eastern reservoir watersheds, while most western reservoirs have non-significant

trends at the annual scale (Figure 21). Seasonally, significantly increasing trends in extreme frequency are most common in the spring, also in central and eastern reservoir watersheds (Figure 22). These patterns are broadly consistent with the east-west gradient in precipitation trends described in Section 2.1.

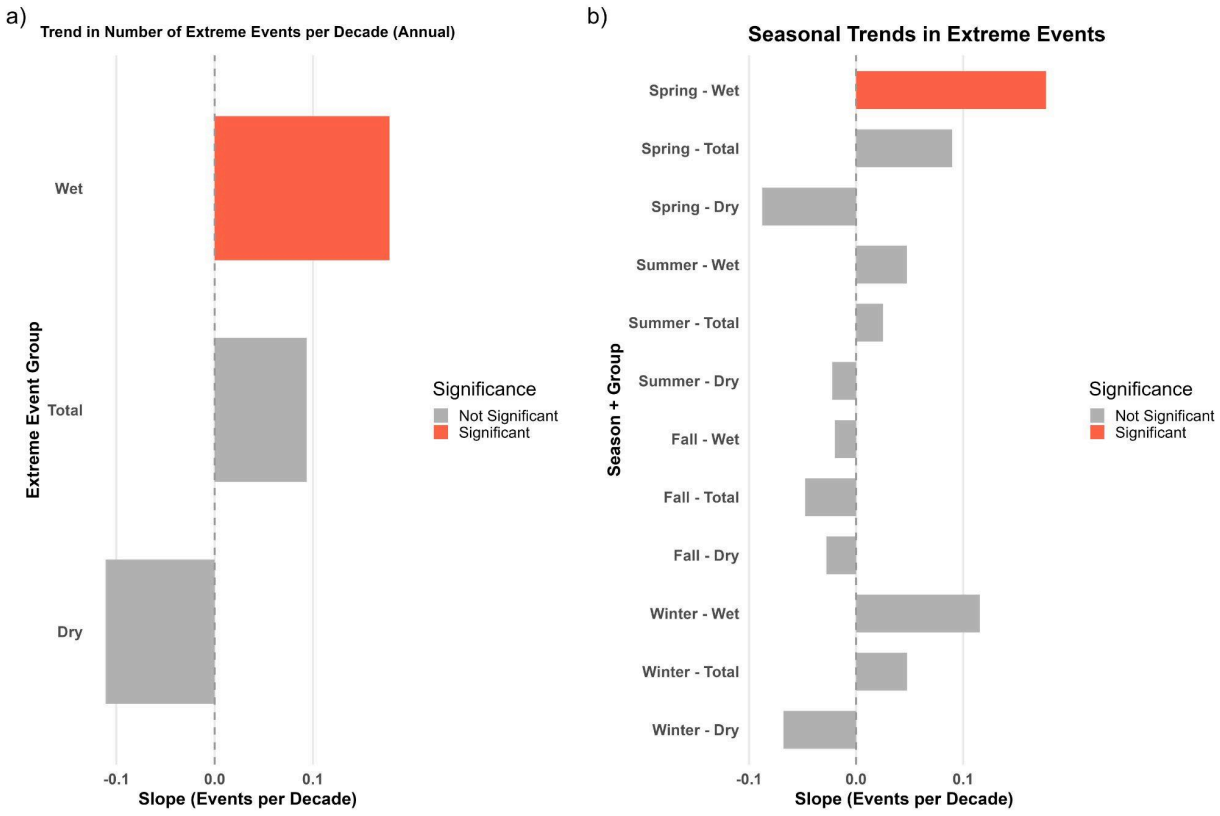

Figure 20. Decadal trends in extreme precipitation event frequency averaged across all Kansas reservoir catchments (1900–2019). (a) Annual trends by event group: wet-type extremes show a significant increasing trend while dry-type extremes show a non-significant decline, and total extremes remain non-significant. (b) Seasonal trends by event group. Bars colored red indicate statistical significance ($p < 0.05$).

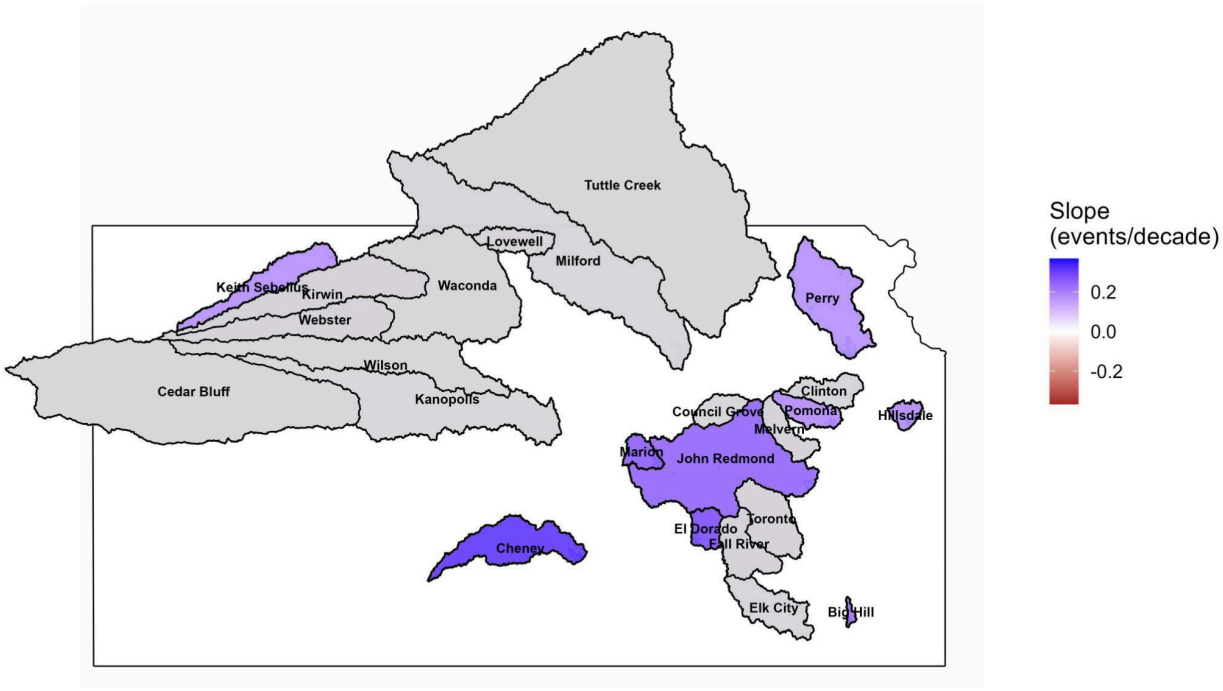

Figure 21. Trend in wet-type extreme event frequency across Kansas reservoir catchments (1900–2019). Color indicates Sen's slope (events per decade); gray catchments indicate non-significant trends ($p \geq 0.05$). Positive values (purple) denote increasing frequency of wet extremes over time.

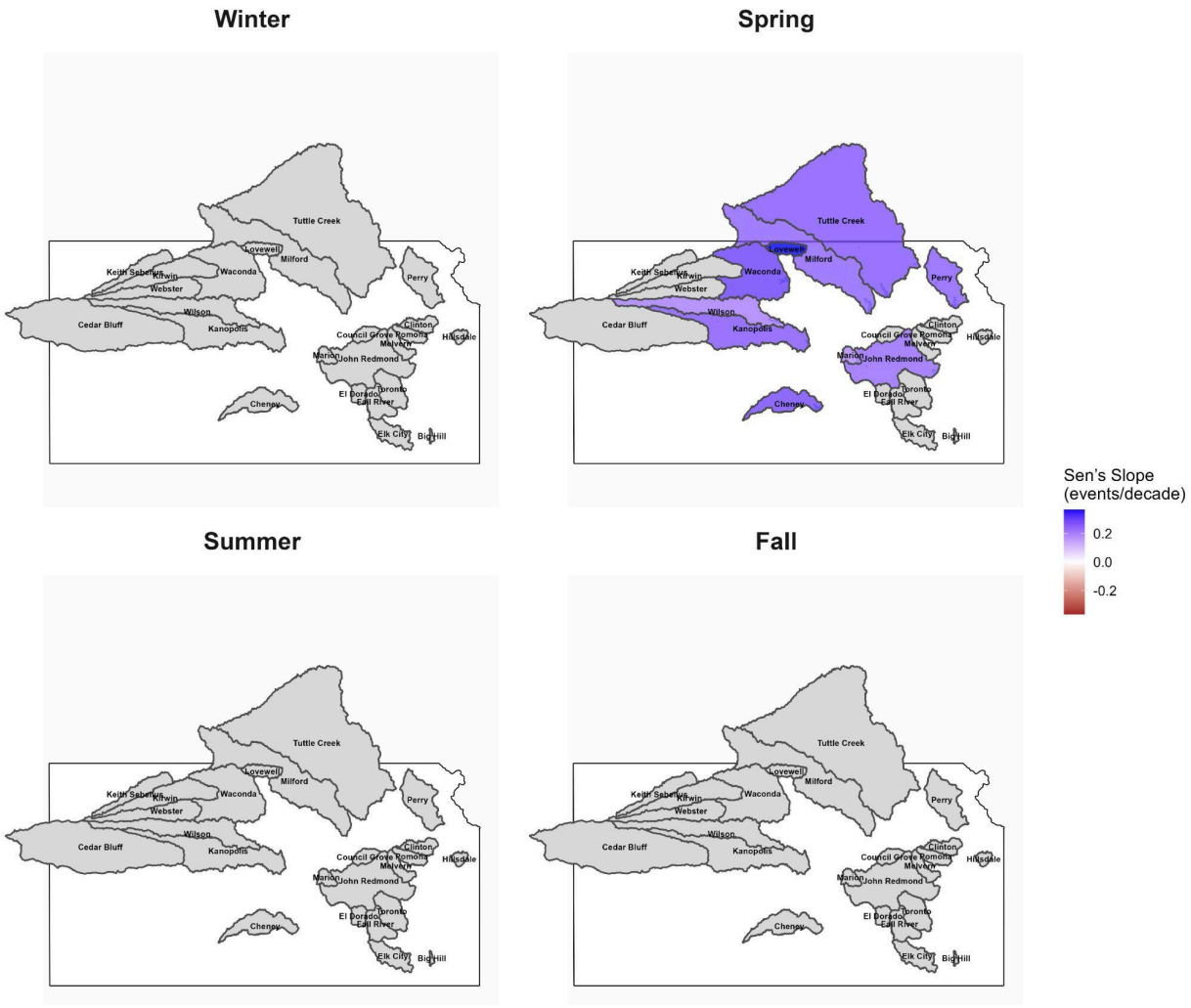

Figure 22. Seasonal trends in wet-type extreme event frequency across Kansas reservoir catchments (1900–2019) for winter, spring, summer, and fall. Color indicates Sen's slope (events per decade); gray catchments are non-significant ($p \geq 0.05$).

As an illustrative example, we show historical dynamics for Cedar Bluff Reservoir (the westernmost watershed, which does not have a significant annual or seasonal trend in extremes) and Cheney Reservoir in south-central Kansas that has significant annual and spring increases in precipitation and wet extremes. The contrast between Cedar Bluff and Cheney illustrates the two ends of this spectrum (Figure 23): Cedar Bluff exhibits subdued interannual variability and infrequent wet extremes throughout the record, while Cheney shows greater variability with an overall increasing annual precipitation trend and many isolated wet and recurring wet-to-wet extremes in recent decades. Seasonal time series (Figures 24–25) further show that differences between the reservoirs are most evident in spring, when central and eastern catchments such as Cheney regularly experience isolated wet and wet-to-wet conditions, while Cedar Bluff remains near-normal across most seasons and years.

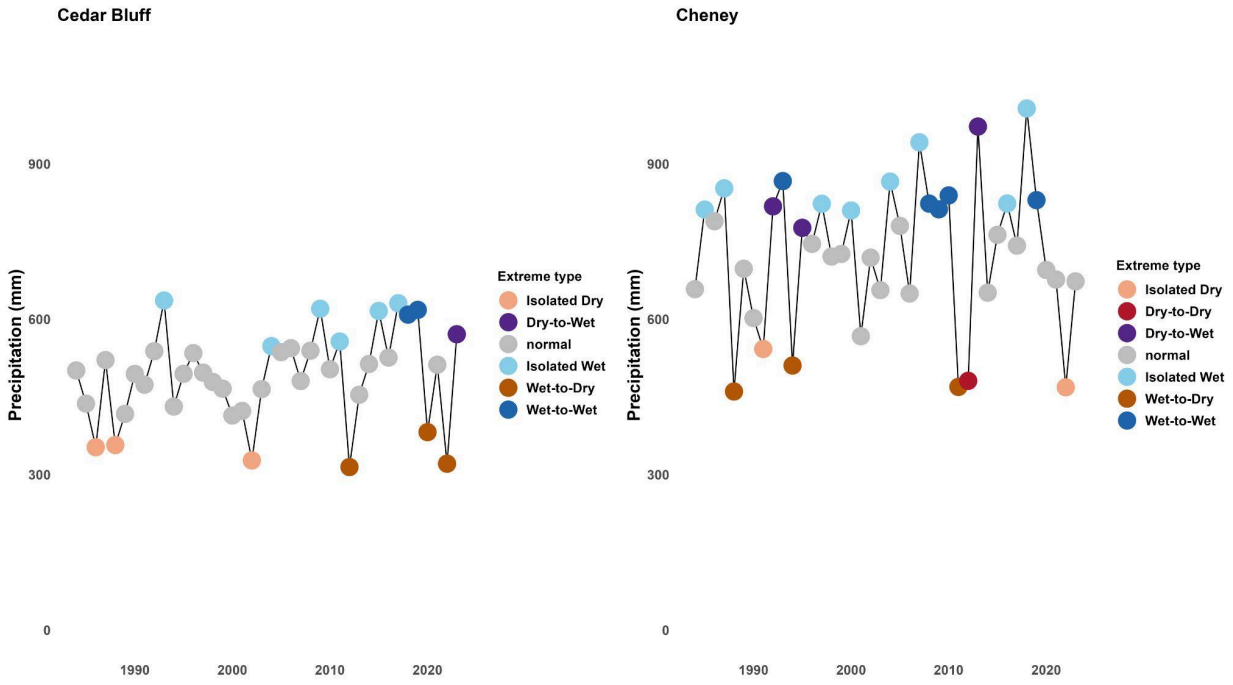

Figure 23. Annual precipitation time series for the Cedar Bluff (western Kansas) and Cheney (central Kansas) Reservoir catchments in the last 40 years of the study period (1984–2023).

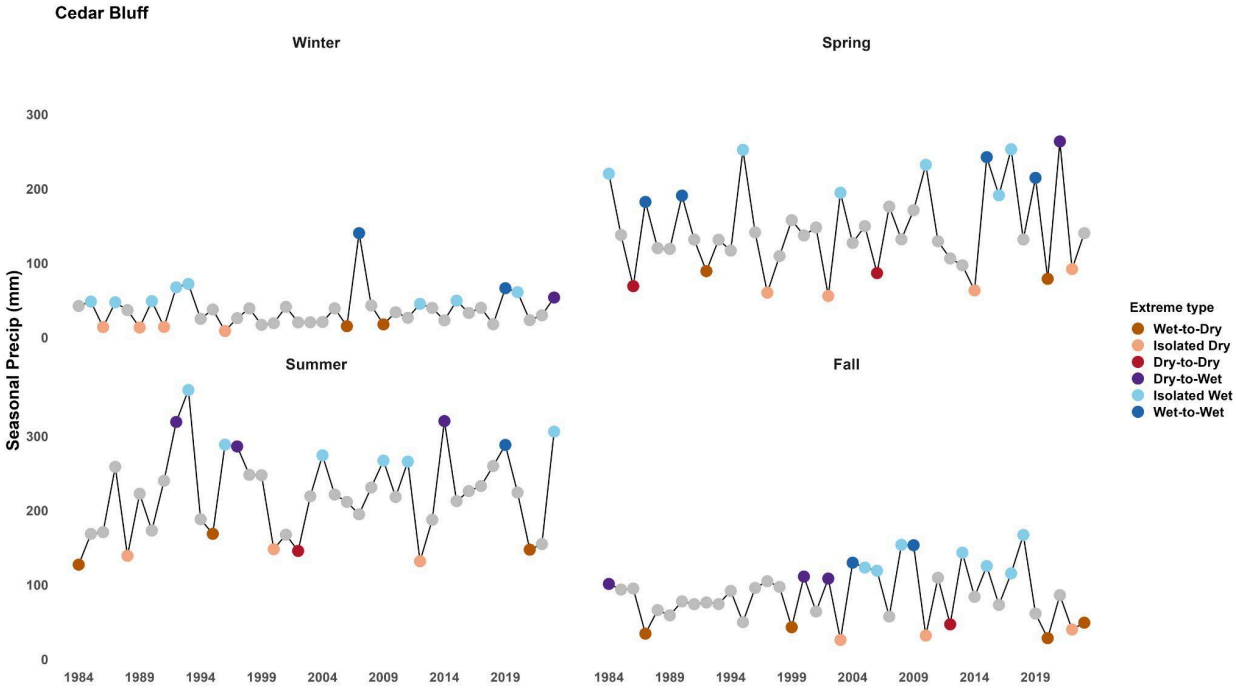

Figure 24. Seasonal precipitation time series for the Cedar Bluff Reservoir catchment in the last 40 years of the study period (1984–2023), shown by winter, spring, summer, and fall.

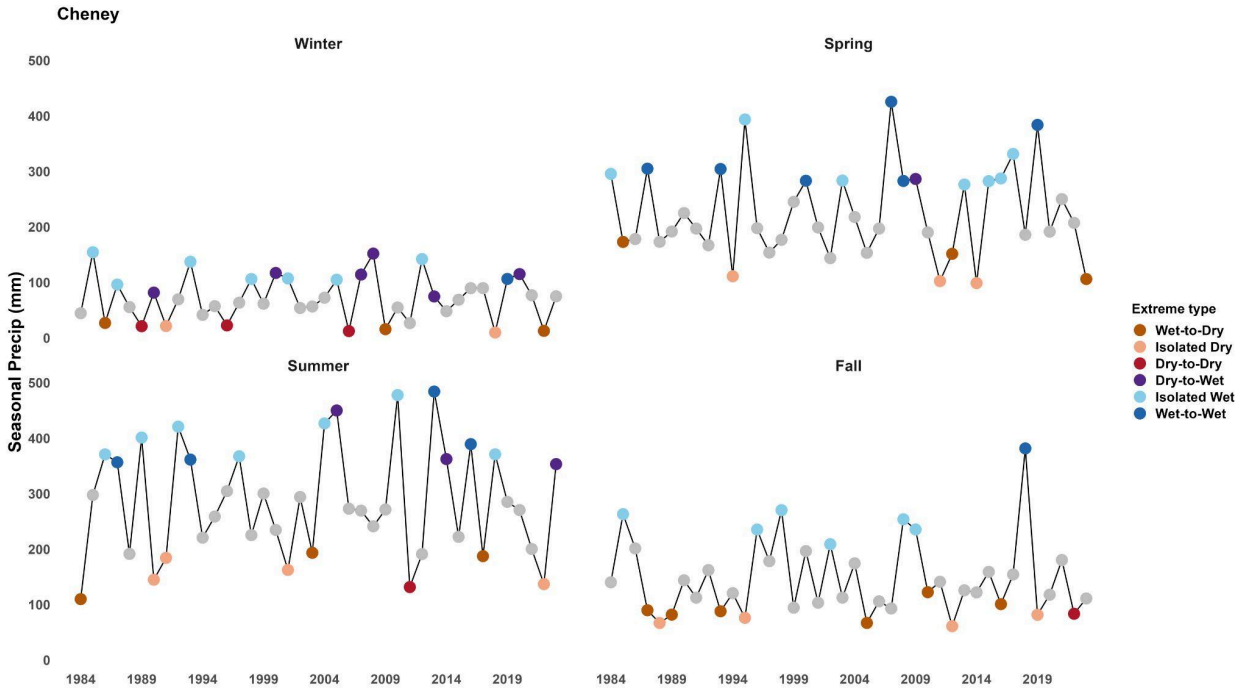

Figure 25. Seasonal precipitation time series for the Cheney Reservoir catchment in the last 40 years of the study period (1984–2023), shown by winter, spring, summer, and fall.

2.3.4 Implications for reservoir sedimentation and management

To examine links between hydroclimatic extremes and reservoir health, we compared the percent capacity lost to sedimentation in each reservoir to the count of wet-type and dry-type extremes since the reservoirs were constructed. The capacity loss data were provided by the Kansas Water Office. Wet-type extreme frequency shows a statistically significant positive relationship with capacity loss (Spearman's $\rho = 0.49$, $p = 0.016$). The relationship between capacity loss and dry-type extremes or years since construction were both positive but not significant (Spearman's $\rho > 0$, $p > 0.05$) (Figure 26). The association between more common wet extremes and greater capacity loss is consistent with the fact that periods of high streamflow can have disproportionately high contributions to sediment loading (deNoyelles and Kastens, 2016; Kramer et al., 2021).

However, we note several confounding factors that preclude us from making a causal relationship between wet extremes and reservoir capacity loss. Reservoir age is one complicating factor, because older reservoirs may have experienced more extreme years and had more time for sediment to accumulate in non-extreme conditions. However, the stronger correlation with wet extremes specifically — rather than with dry extremes or total years of record — supports a process-based interpretation in which high-flow events disproportionately drive sediment delivery and accumulation. Kansas's precipitation gradient is another potential explanatory factor, as reservoirs with more annual precipitation may receive greater average annual inflows of sediment regardless of the presence of extremes. Therefore, while our analysis is not able to

confirm a causal relationship, our results suggest that sedimentation pressures are likely to intensify in coming decades if present trends toward greater annual precipitation and more frequent wet extremes continue across much of the state.

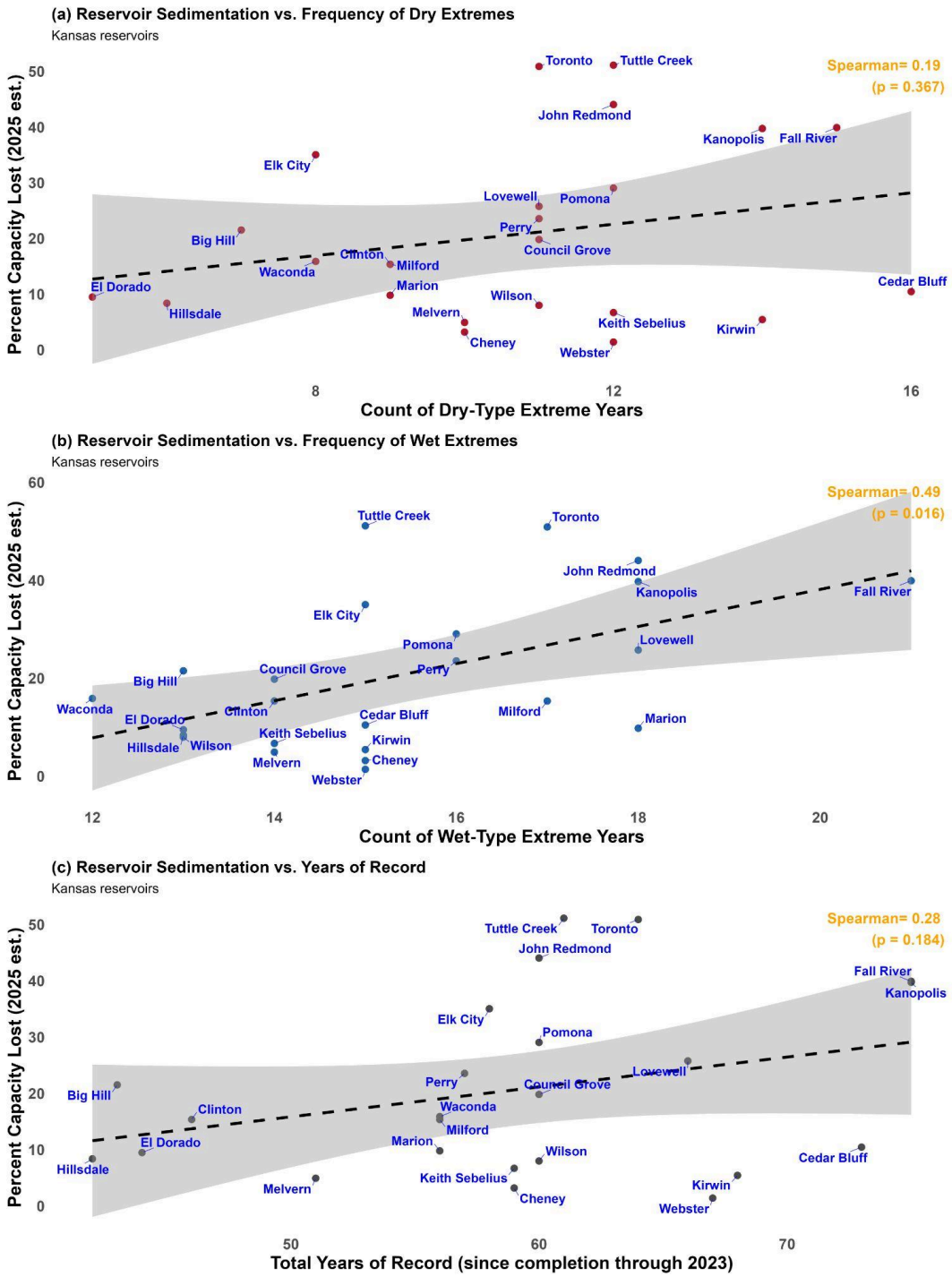

Figure 26. Cumulative frequency of (a) dry-type and (b) wet-type precipitation extremes versus estimated percent capacity lost to sedimentation across Kansas reservoirs (from year of each reservoir's completion through 2023). Panel (c) shows capacity loss as a function of total years since reservoir completion. Dashed lines indicate linear fits with 95% confidence bands. Sedimentation estimates for 23 reservoirs are based on projected 2025 capacity loss data provided by the Kansas Water Office; the Cheney Reservoir estimate uses the 2015 capacity loss value reported in deNoyelles and Kastens (2016).

Objective 3: Develop an interactive, web-based tool for Kansas's hydroclimatic extremes.

3.1 Dashboard design

To support the exploration and dissemination of this project, we developed an interactive, web-based application where users can visualize results for different regions in the state and download data for integration with other data products in their own studies. The tool summarizes data for 148 management-relevant boundaries within the state: 24 federal reservoir watersheds, 5 groundwater management districts, 14 RAC boundaries, and 105 counties. Because of the spatial nature of the analysis, we designed the tool around an interactive map interface that allows users to select an area of interest from these different sets of boundaries, view a series of figures and text summary information, and download data in spreadsheet format.

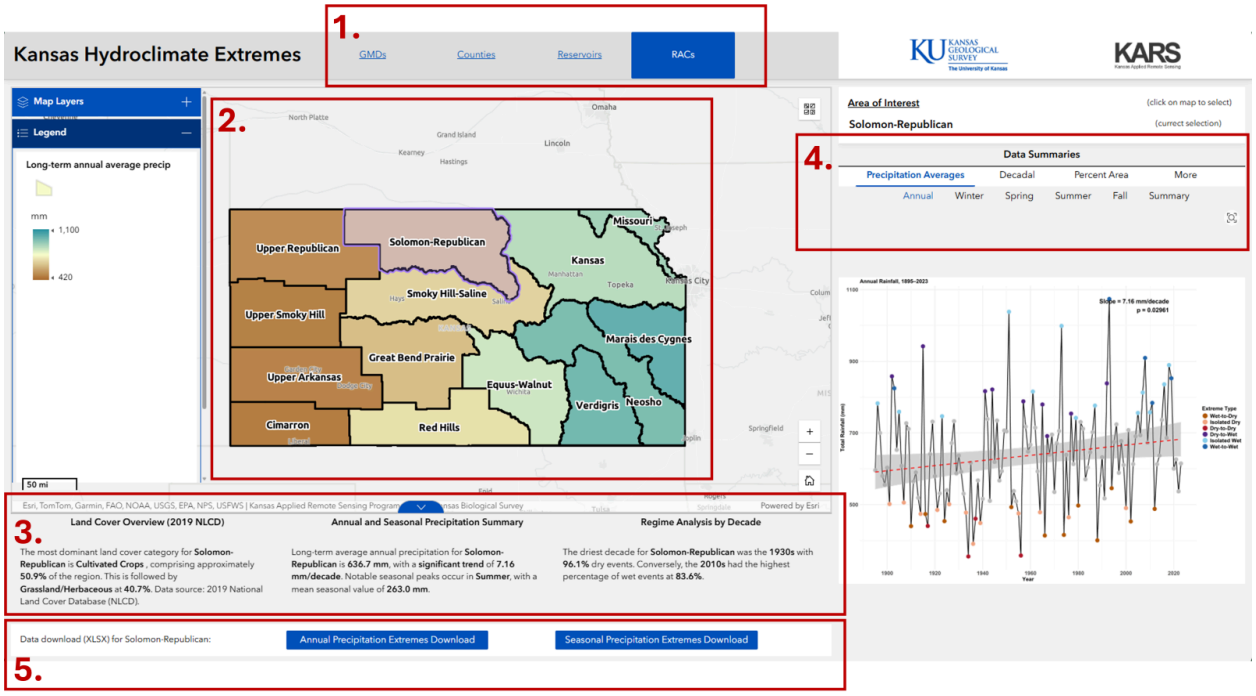

Figure 27. Screenshot of the web application with key features outlined, which are described in the text.

The tool is available online at https://kars.ku.edu/pages/hydroclimate-extremes, and Figures 27 and 28 show screenshots. Key features annotated on these screenshots include:

1. The header tab contains buttons to navigate between management area types (GMDs, RACs, reservoir watersheds, and counties).
2. An interactive map shows the management unit boundaries and, upon selection by click, updates the contents of panes 3 (summary narrative), 4 (figure viewer), and 5 (download links) to the selected area of interest.

3. The summary narratives section provides information about land cover, long-term climate, and historical extreme regime analysis. Land cover information includes the two most frequently occurring land cover classifications for the area according to the 2019 National Land Cover Database. Long-term climate highlights the long-term annual average precipitation trend and peak season. Historical extreme regime analysis summarizes the driest and wettest decades.
4. The Data Summaries figure viewer presents graphs characterizing the management unit's precipitation averages and trends, decadal extreme event distributions, and percent area by event type. Different graphs can be selected by clicking on various headers within the Data Summaries section.
5. The data download pane at the bottom has download links for the annual precipitation and seasonal precipitation extremes spreadsheets, summarized for the region.
6. The map frame allows the viewer to select different layers to visualize long-term annual average precipitation (default), wettest and driest decades, and the National Land Cover Database land cover.

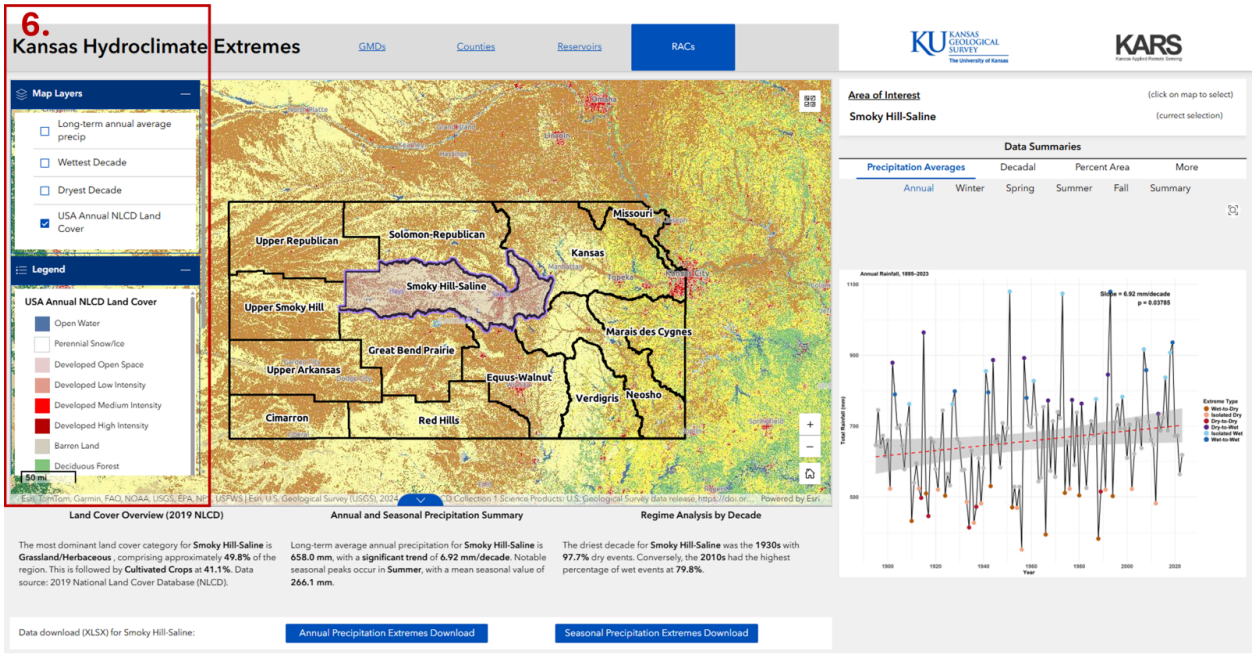

Figure 28. Screenshot of alternate view of web application with key features outlined (features are described in the text). This view shows the ability to change map layers that visualize different spatial datasets.

3.2 Technical details and design considerations

The tool is built with the ESRI Experience Builder platform. The management unit boundary layers have attribute tables that contain columns for dynamic text items, links for each figure, and links for the spreadsheet downloads. Figures, spreadsheets, and the management unit boundary layers are hosted on Kansas Applied Remote Sensing's geospatial server.

Priorities included ease of use, design that allows for comparison across management subunits, efficient server and client resource use, and minimal maintenance. To address the first two concerns, we structured the application for uniformity across the four management area types and organized the figures by category with subdivision by temporal extent. The figure viewer remains on the last selected figure type while navigating management subunits to facilitate comparison. Serving static figures rather than rendering interactive figures avoids the need to generate data summaries and visualizations on demand, which would increase both server and client-side load. Figure design constraints of the standard Experience Builder platform also precluded the latter approach.

The Developer Edition of Experience Builder offers greater flexibility and customization than the standard version but is more maintenance-intensive and necessitates programming skill to update and troubleshoot. Using the standard version required some workarounds to accommodate the application's complexity and achieve the design goals. The most significant workaround involved separating each management area type's page into its own Experience Builder application and using hyperlink buttons in the header tab intended to look and behave like a menu in a single application.

References

Bolles, K. C., and Forman, S. L., 2018, Evaluating Landscape Degradation Along Climatic Gradients During the 1930s Dust Bowl Drought From Panchromatic Historical Aerial Photographs, United States Great Plains: Frontiers in Earth Science, v. 6. https://doi.org/10.3389/feart.2018.00153.

Daly, C., Halbleib, M., Smith, J. I., Gibson, W. P., Doggett, M. K., Taylor, G. H., Curtis, J., and Pasteris, P. P., 2008, Physiographically sensitive mapping of climatological temperature and precipitation across the conterminous United States: International Journal of Climatology, v. 28, no. 15, p. 2031–2064. https://doi.org/10.1002/joc.1688.

Datry, T., Truchy, A., Olden, J. D., Busch, M. H., Stubbington, R., Dodds, W. K., Zipper, S., Yu, S., Messager, M. L., Tonkin, J. D., Kaiser, K. E., Hammond, J. C., Moody, E. K., Burrows, R. M., Sarremejane, R., DelVecchia, A. G., Fork, M. L., Little, C. J., Walker, R. H., Walters, A. W., and Allen, D., 2022, Causes, Responses, and Implications of Anthropogenic versus Natural Flow Intermittence in River Networks: BioScience, p. biac098. https://doi.org/10.1093/biosci/biac098.

deNoyelles, F., and Kastens, J. H., 2016, Reservoir Sedimentation Challenges in Kansas: Transactions of the Kansas Academy of Science, v. 119, no. 1, p. 69–81. https://doi.org/10.1660/062.119.0110.

Di Baldassarre, G., Wanders, N., AghaKouchak, A., Kuil, L., Rangecroft, S., Veldkamp, T. I. E., Garcia, M., Oel, P. R. van, Breinl, K., and Loon, A. F. V., 2018, Water shortages worsened by reservoir effects: Nature Sustainability, v. 1, no. 11, p. 617. https://doi.org/10.1038/s41893-018-0159-0.

Di Capua, G., and Rahmstorf, S., 2023, Extreme weather in a changing climate: Environmental Research Letters, v. 18, no. 10, p. 102001. https://doi.org/10.1088/1748-9326/acfb23.

Easterling, D. R., Kunkel, K. E., Wehner, M. F., and Sun, L., 2016, Detection and attribution of climate extremes in the observed record: Weather and Climate Extremes, v. 11, p. 17–27. https://doi.org/10.1016/j.wace.2016.01.001.

Fowler, K., Peel, M., Saft, M., Nathan, R., Horne, A., Wilby, R., McCutcheon, C., and Peterson, T., 2022, Hydrological Shifts Threaten Water Resources: Water Resources Research, v. 58, no. 8, p. e2021WR031210. https://doi.org/10.1029/2021WR031210.

Fraser, E. D. G., 2013, Coping with food crises: Lessons from the American Dust Bowl on balancing local food, agro technology, social welfare, and government regulation agendas in food and farming systems: Global Environmental Change-Human and Policy Dimensions, v. 23, no. 6, p. 1662–1672. https://doi.org/10.1016/j.gloenvcha.2013.09.001.

Fu, J., Lu, Y., Liu, B., Tan, X., Wei, J., Tan, X., Huang, Z., and Chen, X., 2025, Intensifying Hydroclimate Whiplash From a 3D Perspective: Water Resources Research, v. 61, no. 11, p. e2025WR040607. https://doi.org/10.1029/2025WR040607.

Gründemann, G. J., Zorzetto, E., van de Giesen, N., and van der Ent, R. J., 2023, Historical Shifts in Seasonality and Timing of Extreme Precipitation: Geophysical Research Letters, v. 50, no. 24, p. e2023GL105200. https://doi.org/10.1029/2023GL105200.

He, X., and Sheffield, J., 2020, Lagged Compound Occurrence of Droughts and Pluvials Globally Over the Past Seven Decades: Geophysical Research Letters, v. 47, no. 14. https://doi.org/10.1029/2020gl087924.

Houspanossian, J., Giménez, R., Whitworth-Hulse, J. I., Nosetto, M. D., Tych, W., Atkinson, P. M., Rufino, M. C., and Jobbágy, E. G., 2023, Agricultural expansion raises groundwater and increases flooding in the South American plains: Science, v. 380, no. 6652, p. 1344–1348. https://doi.org/10.1126/science.add5462.

Kitoh, A., Endo, H., Krishna Kumar, K., Cavalcanti, I. F. A., Goswami, P., and Zhou, T., 2013, Monsoons in a changing world: A regional perspective in a global context: Journal of Geophysical Research: Atmospheres, v. 118, no. 8, p. 3053–3065. https://doi.org/10.1002/jgrd.50258.

Kramer, A. R., Peterman-Phipps, C. L., Mahoney, M. D., and Lukasz, B. S., 2021, Sediment concentrations and loads upstream from and through John Redmond Reservoir, east-central Kansas, 2010–19: U.S. Geological Survey, 2021–5037.

Kuil, L., Carr, G., Viglione, A., Prskawetz, A., and Blöschl, G., 2016, Conceptualizing socio-hydrological drought processes: The case of the Maya collapse: Water Resources Research, v. 52, no. 8, p. 6222–6242. https://doi.org/10.1002/2015WR018298.

Li, X., Mann, M. E., Wehner, M. F., and Christiansen, S., 2025, Increased frequency of planetary wave resonance events over the past half-century: Proceedings of the National Academy of Sciences, v. 122, no. 25, p. e2504482122. https://doi.org/10.1073/pnas.2504482122.

Lin, X., Harrington, J., Ciampitti, I., Gowda, P., Brown, D., and Kisekka, I., 2017, Kansas Trends and Changes in Temperature, Precipitation, Drought, and Frost-Free Days from the 1890s to 2015: Journal of Contemporary Water Research & Education, v. 162, no. 1, p. 18–30. https://doi.org/10.1111/j.1936-704X.2017.03257.x.

Loecke, T. D., Burgin, A. J., Riveros-Iregui, D. A., Ward, A. S., Thomas, S. A., Davis, C. A., and Clair, M. A. S., 2017, Weather whiplash in agricultural regions drives deterioration of water quality: Biogeochemistry, p. 1–9. https://doi.org/10.1007/s10533-017-0315-z.

Na, W., and Najafi, M. R., 2024, Rising risks of hydroclimatic swings: A large ensemble study of dry and wet spell transitions in North America: Global and Planetary Change, v. 238, p. 104476. https://doi.org/10.1016/j.gloplacha.2024.104476.

Overpeck J, and Udall B., 2010, Dry times ahead: Science, v. 328, no. 5986, p. 1642-1643. https://doi.org/10.1126/science.1186591

Perkin, J. S., Starks, T. A., Pennock, C. A., Gido, K. B., Hopper, G. W., and Hedden, S. C., 2019, Extreme drought causes fish recruitment failure in a fragmented Great Plains riverscape: Ecohydrology, p. e2120. https://doi.org/10.1002/eco.2120.

Preota, S. A., Talukdar, G., and Zipper, S., 2025, Evaluating annual precipitation extremes in the U.S. Great Plains using PRISM data: Kansas Geological Survey, KGS Open-File Report 2025–1.

Reyes, J., Elias, E., Haacker, E., Kremen, A., Parker, L., and Rottler, C., 2020, Assessing agricultural risk management using historic crop insurance loss data over the Ogallala Aquifer: Agricultural Water Management, v. 232, p. 106000. https://doi.org/10.1016/j.agwat.2020.106000.

Rogosch, J. S., Tonkin, J. D., Lytle, D. A., Merritt, D. M., Reynolds, L. V., and Olden, J. D., 2019, Increasing drought favors nonnative fishes in a dryland river: evidence from a multispecies demographic model: Ecosphere, v. 10, no. 4, p. e02681. https://doi.org/10.1002/ecs2.2681.

Seager, R., Lis, N., Feldman, J., Ting, M., Williams, A. P., Nakamura, J., Liu, H., and Henderson, N., 2017, Whither the 100th Meridian? The Once and Future Physical and Human Geography of America's Arid–Humid Divide. Part I: The Story So Far: Earth Interactions, v. 22, no. 5, p. 1–22. https://doi.org/10.1175/EI-D-17-0011.1.

Smith, E., Grant, N., Luo, X., and Diaz, D., 2025, Evaluating the ability of gridded climate datasets to capture temperature and precipitation trends and extremes: Scientific Reports, v. 15, 12607. https://doi.org/10.1038/s41598-025-97570-7

Swain, D. L., Langenbrunner, B., Neelin, J. D., and Hall, A., 2018, Increasing precipitation volatility in twenty-first-century California: Nature Climate Change, v. 8, no. 5, p. 427–433. https://doi.org/10.1038/s41558-018-0140-y.

Swain, D. L., Prein, A. F., Abatzoglou, J. T., Albano, C. M., Brunner, M., Diffenbaugh, N. S., Singh, D., Skinner, C. B., and Touma, D., 2025, Hydroclimate volatility on a warming Earth: Nature Reviews Earth & Environment, v. 6, no. 1, p. 35–50. https://doi.org/10.1038/s43017-024-00624-z.

Tramblay, Y., Arnaud, P., Artigue, G., Lang, M., Paquet, E., Neppel, L., and Sauquet, E., 2023, Changes in Mediterranean flood processes and seasonality: Hydrology and Earth System Sciences, v. 27, no. 15, p. 2973–2987. https://doi.org/10.5194/hess-27-2973-2023.

Yuan, X., Wang, Y., Ji, P., Wu, P., Sheffield, J., and Otkin, J. A., 2023, A global transition to flash droughts under climate change: Science, v. 380, no. 6641, p. 187–191. https://doi.org/10.1126/science.abn6301.

Zhao, C., Brissette, F., Chen, J., and Martel, J.-L., 2020, Frequency change of future extreme summer meteorological and hydrological droughts over North America: Journal of Hydrology, v. 584, p. 124316. https://doi.org/10.1016/j.jhydrol.2019.124316.

Zipper, S. C., Hammond, J. C., Shanafield, M., Zimmer, M., Datry, T., Jones, C. N., Kaiser, K. E., Godsey, S. E., Burrows, R. M., Blaszczak, J. R., Busch, M. H., Price, A. N., Boersma, K. S., Ward, A. S., Costigan, K., Allen, G. H., Krabbenhoft, C. A., Dodds, W. K., Mims, M. C., Olden,

J. D., Kampf, S. K., Burgin, A. J., and Allen, D. C., 2021, Pervasive changes in stream intermittency across the United States: Environmental Research Letters, v. 16, no. 8, p. 084033. https://doi.org/10.1088/1748-9326/ac14ec.

Zipper, S., Popescu, I., Compare, K., Zhang, C., and Seybold, E. C., 2022, Alternative stable states and hydrological regime shifts in a large intermittent river: Environmental Research Letters, v. 17, p. 074005. https://doi.org/10.1088/1748-9326/ac7539.

Appendix 1: Comparison of PRISM and station-based precipitation data and extreme identification

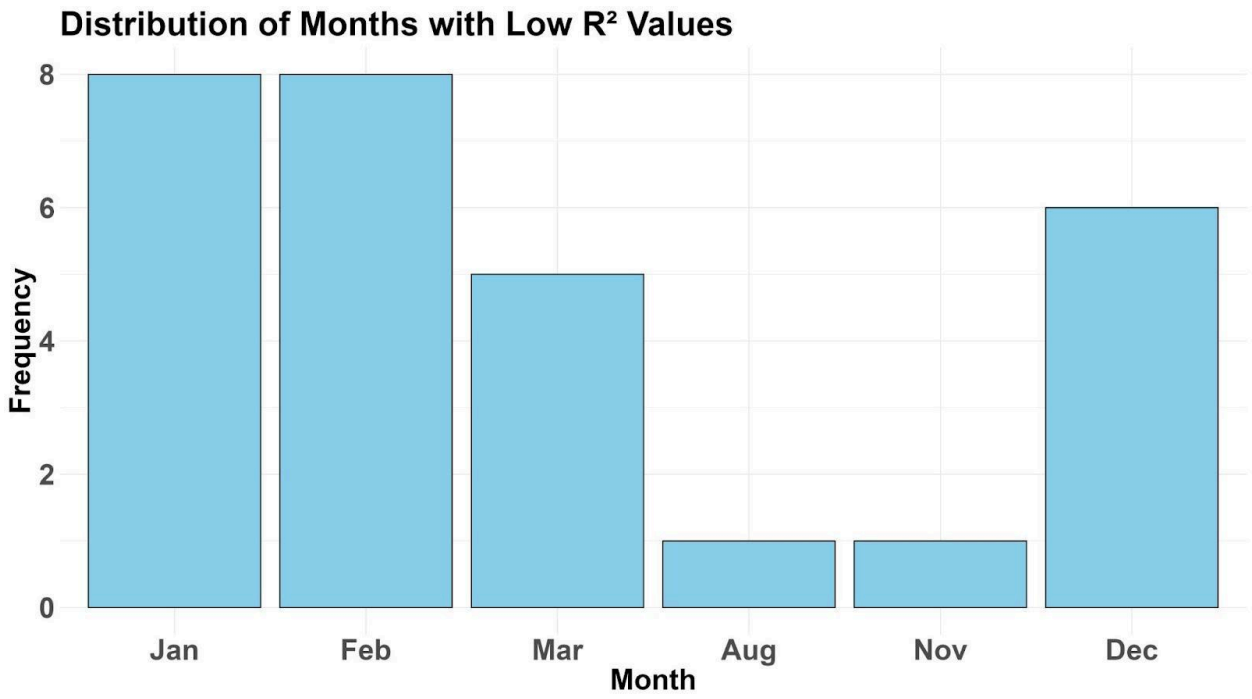

Figure A1. Distribution of months with low correlation ($R^2 < 0.6$) between PRISM and station precipitation data across 22 stations.

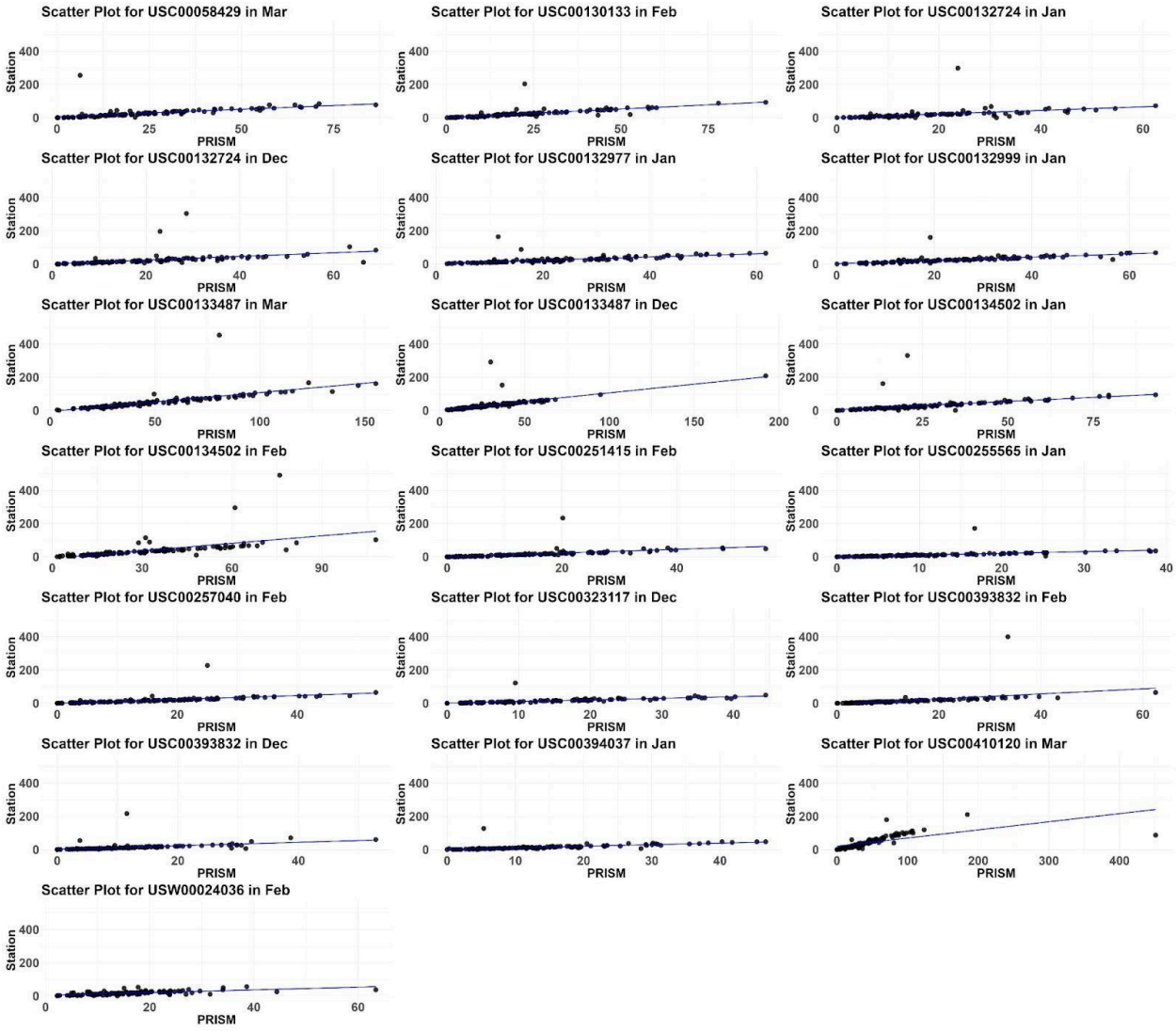

Figure A2. Scatter plots of total monthly precipitation recorded at weather stations versus PRISM-derived precipitation for months and stations where the correlation coefficient (R^2) falls below 0.5. Each plot represents a different station-month combination, with station-measured precipitation (y-axis) compared against PRISM-estimated precipitation (x-axis). The blue line represents the linear regression fit for each dataset.

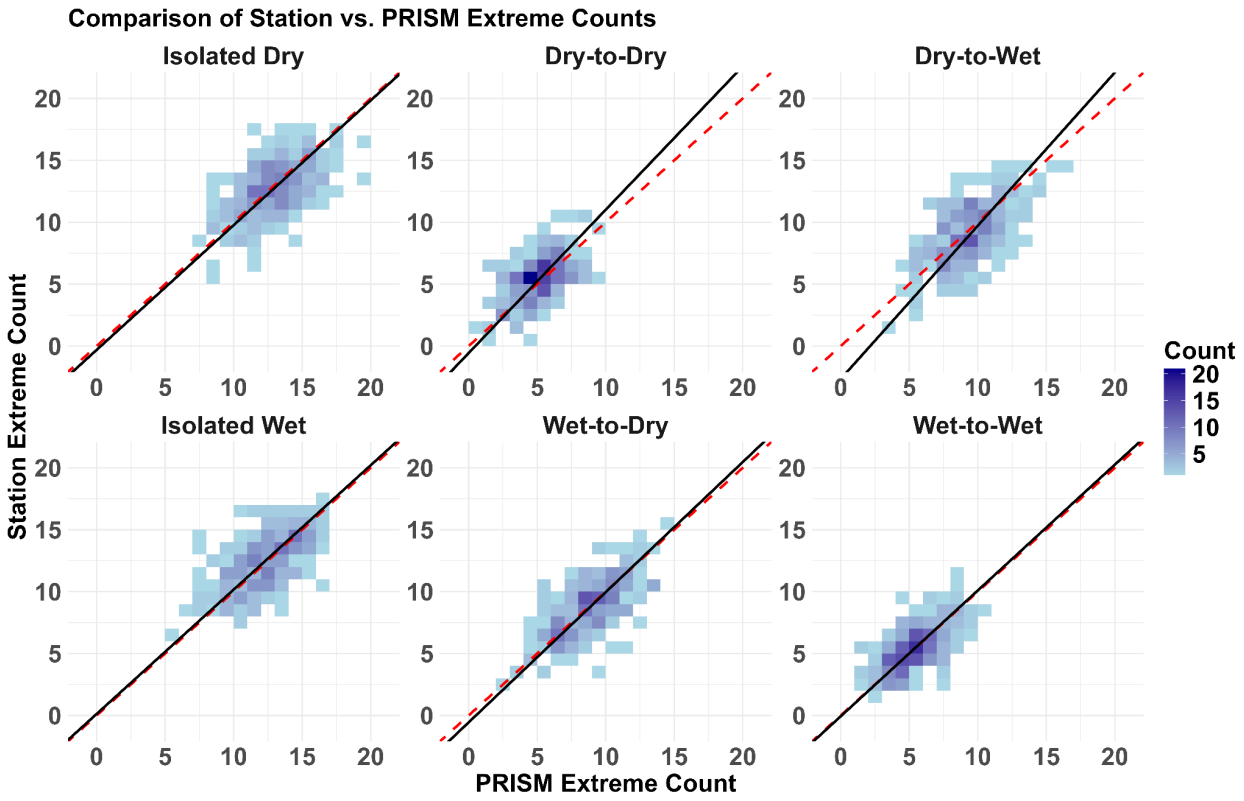

Figure A3. Comparison of extreme event counts between PRISM estimates and station annual observations (1895–2023) across different extreme transition types. The graph represents the density of data points, with darker blue shades indicating higher densities. The red dashed line represents the 1:1 relationship, where PRISM and station counts are equal. The black solid line represents the best-fit total least squares regression line, indicating the observed relationship between the two datasets. The panels correspond to different extreme transition types, including dry, wet, and transition events (e.g., dry-to-wet, wet-to-dry).

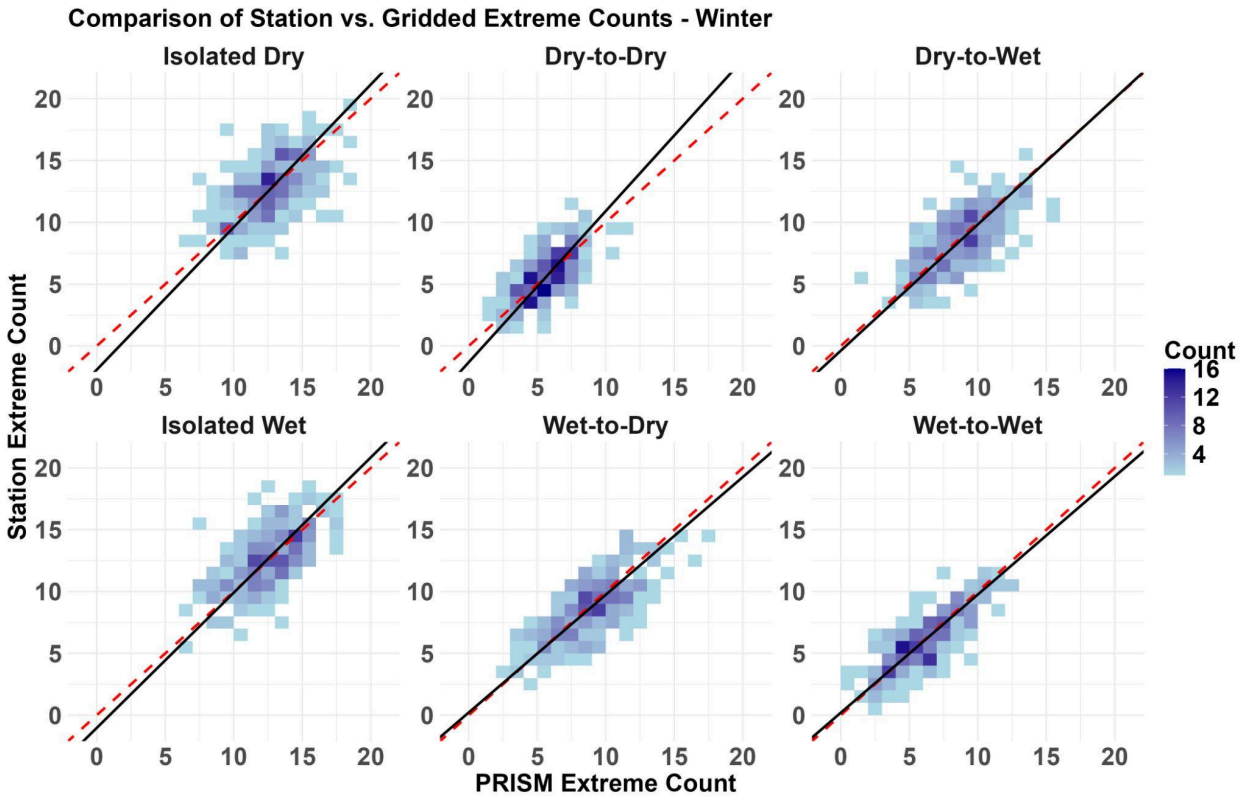

Figure A4. Comparison of extreme event counts derived from station observations and gridded PRISM data for the winter season (March 1895–May 2024). The heatmap represents the density of data points, with darker blue shades indicating higher density. The red dashed line represents the 1:1 reference line, where station and gridded counts would be equal. The black solid line represents the best-fit total least squares regression line, illustrating the relationship between station-based and gridded extreme event counts for different transition types.

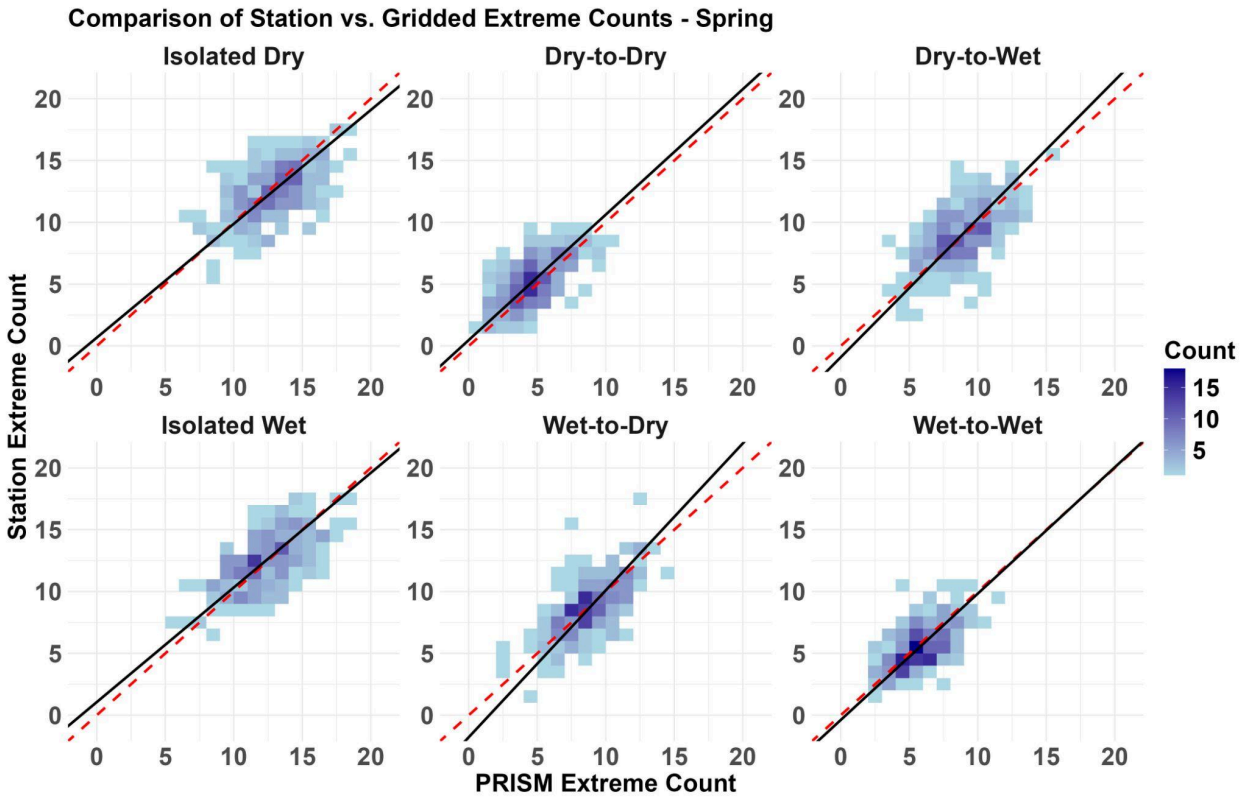

Figure A5. Comparison of extreme event counts derived from station observations and gridded PRISM data for the spring season (March 1895–May 2024). The heatmap represents the density of data points, with darker blue shades indicating higher density. The red dashed line represents the 1:1 reference line, where station and gridded counts would be equal. The black solid line represents the best-fit total least squares regression line, illustrating the relationship between station-based and gridded extreme event counts for different transition types.

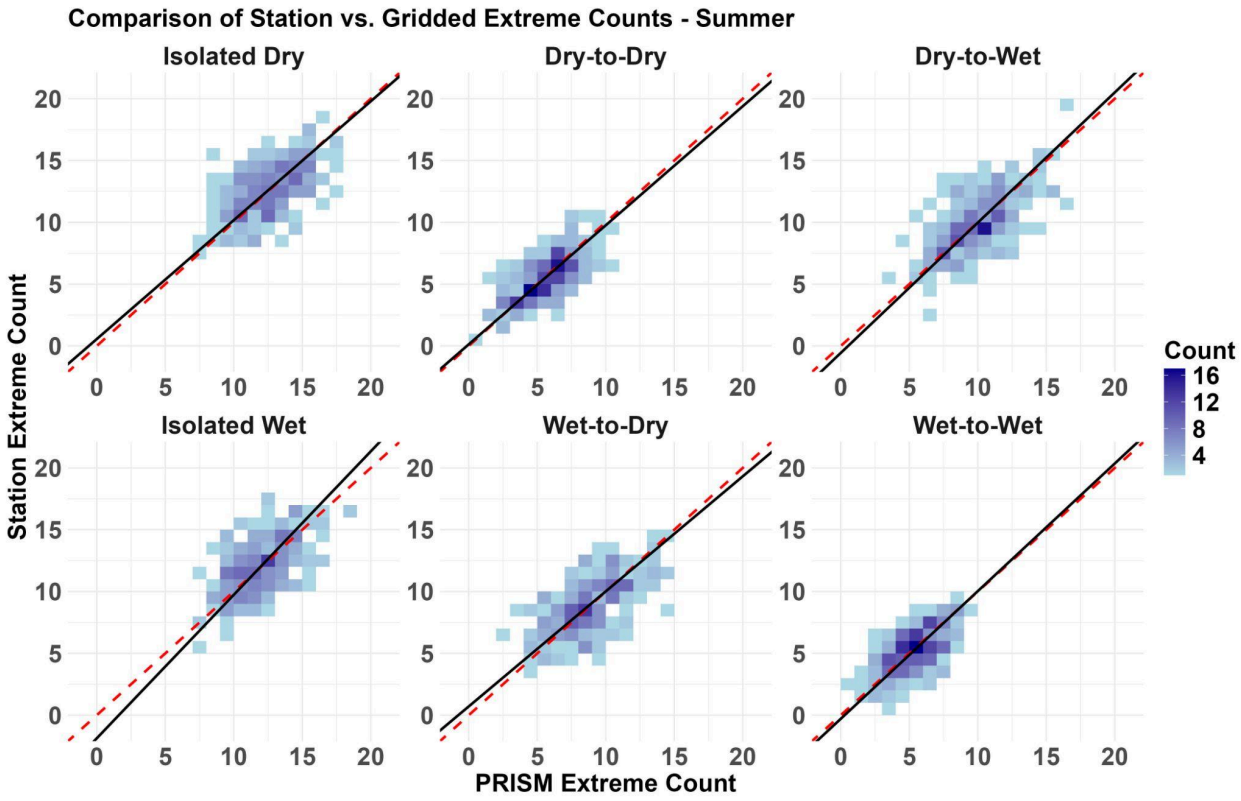

Figure A6. Comparison of extreme event counts derived from station observations and gridded PRISM data for the summer season (March 1895–May 2024). The heatmap represents the density of data points, with darker blue shades indicating higher density. The red dashed line represents the 1:1 reference line, where station and gridded counts would be equal. The black solid line represents the best-fit total least squares regression line, illustrating the relationship between station-based and gridded extreme event counts for different transition types.

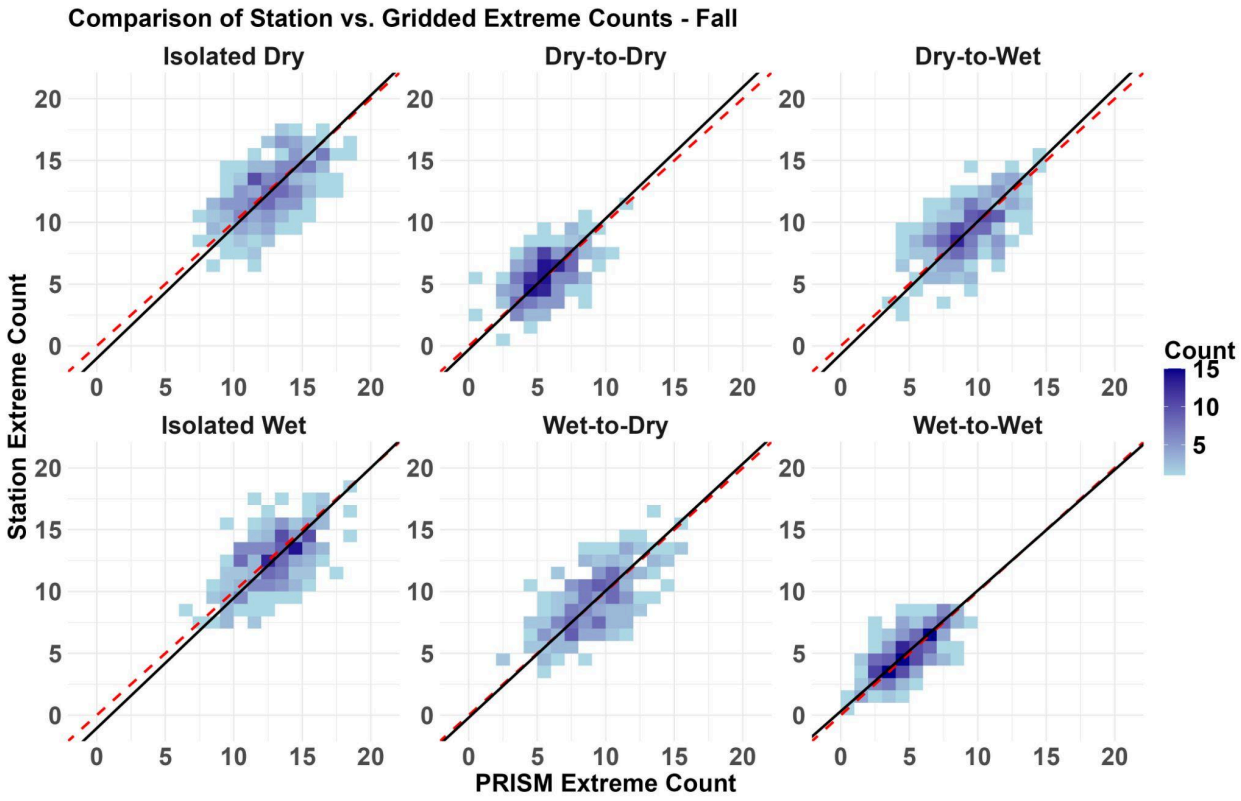

Figure A7. Comparison of extreme event counts derived from station observations and gridded PRISM data for the fall season (March 1895–May 2024). The heatmap represents the density of data points, with darker blue shades indicating higher density. The red dashed line represents the 1:1 reference line, where station and gridded counts would be equal. The black solid line represents the best-fit total least squares regression line, illustrating the relationship between station-based and gridded extreme event counts for different transition types.